Temperature trends and variability in the Greater Horn of Africa: interactions with precipitation.

Pierre Camberlin

▶ **To cite this version:**

Pierre Camberlin. Temperature trends and variability in the Greater Horn of Africa: interactions with precipitation.. Climate Dynamics, 2017, 48 (1-2), pp.477-498. 10.1007/s00382-016-3088-5 . hal-01477164

HAL Id: hal-01477164
https://hal.science/hal-01477164

Submitted on 8 Feb 2024

HAL is a multi-disciplinary open access archive for the deposit and dissemination of scientific research documents, whether they are published or not. The documents may come from teaching and research institutions in France or abroad, or from public or private research centers.

L'archive ouverte pluridisciplinaire **HAL**, est destinée au dépôt et à la diffusion de documents scientifiques de niveau recherche, publiés ou non, émanant des établissements d'enseignement et de recherche français ou étrangers, des laboratoires publics ou privés.

Temperature trends and variability in the Greater Horn of Africa : interactions with precipitation

Pierre Camberlin[(1)]

(1) Centre de Recherches de Climatologie / Biogéosciences,
UMR 6282 CNRS – Univ. Bourgogne Franche-Comté, F-21000 Dijon
pierre.camberlin@u-bourgogne.fr

Submitted to :

Climate Dynamics

23 November 2015

Revised version 19 February 2016

Abstract

Relationships between daily precipitation and daily maximum and minimum temperature (Tx and Tn, respectively) are analyzed at station level over the Greater Horn of Africa (GHA). Rainfall occurrence is associated with either above normal Tn (mostly in cool highland areas) or below normal Tn (especially lowland, hot environments and early parts of the rainy season). Tx generally displays a more consistent response to rainfall occurrence, with cooling peaking one day after the rainfall event. However there is often a persistence of this cooling several days after the rainfall event, and the amplitude of the cooling is also greater for heavy rainfall events. These temperature anomalies are thought to be a response to cloudiness (concurrent reduced Tx and concurrent enhanced Tn) and soil moisture (reduced Tx and Tn, suggested to reflect evaporative cooling).

These relationships are of relevance to the interpretation of temperature trends. From 1973 to 2013, the GHA shows a clear warming signal, for both Tn (+0.20 to +0.25°C/decade depending on seasons) and Tx (+0.17 to +0.22°C/decade). Rainfall shows both negative (mostly between February and July) and positive trends (mostly in October-December). Given the superimposition of temperature and rainfall trends in parts of the GHA and the covariations between daily rainfall and both Tx and Tn, regression models are used to extract the rainfall influence on temperature, accounting for lag effects up to 4 days. The daily residuals from these models are used to depict temperature variations free from precipitation effects. At some stations, trends computed on these residuals noticeably differ from the raw Tx trends. When averaged across the GHA, these effects do not exceed -0.06 to +0.03°C/decade (depending on the month) for Tx, and are marginal for Tn, thus do not strongly modify the magnitude of the warming in the last 40 years. Nevertheless, these results show that precipitation-temperature relationships must be addressed when analyzing temperature changes.

Keywords:

Temperature; rainfall; eastern Africa; trends; warming

1. Introduction

Many factors are involved in temporal temperature variations, both high- and low-frequency, and they often interact with each other. The attribution of global temperature change to anthropogenic factors is undisputed, but at regional or local scale the interpretation of observed trends in temperature is more complex. Anthropogenic trends, caused by enhanced global GHG concentrations or local land use changes, may be altered by decadal-scale natural climate variability, and in both cases the respective parts played by radiative and advective processes is often poorly known. In particular, the exact role of clouds is still unclear (Soden and Held 2006 ; Boé and Terray 2013). Beyond the complex issue of the influence of atmospheric composition changes on cloud formation, clouds themselves have a decisive effect on surface temperature. This influence is strongest at sub-daily time-scales, and the direction of this effect often differs between day and night (Groisman et al. 2000 ; Sun et al. 2000). Day-time cloud cover decreases incoming shortwave radiation, which therefore results, in places and seasons where temperature is dominantly controlled by the radiative balance, in lower temperatures than under clear sky conditions. It is expected that night-time cloud cover results in higher than normal temperature due to the reduction of outgoing terrestrial radiation. However, several factors (combination of cloud cover with warm or cold air advection, types and height of clouds…) make the relationship between temperature and cloudiness strongly space- and time-dependent.

At interannual time-scales, several studies have shown that the temperature-cloudiness relationship is relatively strong in many places of the world. Tang et al. (2012) and Tang and Leng (2012a) found that the variance of European and North America summer temperature is partly explained by changes in cloudiness. Tang and Leng (2012b) showed evidence that in parts of Eurasia the interaction between daytime cloud cover and surface air temperature was strong enough to influence long-term trends in summer temperature change. Liu et al. (2008) noted that under an assumption of a temperature difference of -7K between cloudy and clear conditions, the effect of changes in cloud cover on regional temperature trends is non negligible. However, the question of temperature-cloudiness relationships is compounded by the paucity of reliable cloud cover data for the last decades, due to the reduction of manned observations in some regions (Dai et al. 2006) and the artifacts found in satellite products (Evan et al. 2007).

A way to overcome this issue is to use precipitation data. Although precipitation cannot be readily considered as a true proxy for cloudiness, it has several advantages. First, rainfall data are available at a much denser network of stations and over longer periods than cloudiness data. Second, studying the relationship between temperature and precipitation enables to indirectly address both the cooling / warming effects of cloudiness and the cooling effects of surface moisture evaporation after a rainfall event. Soil moisture has actually been shown to impact heat wave occurrence in Europe (Fischer et al. 2007 ; Hirschi et al. 2011). The global effects of precipitation, cloudiness and soil moisture on diurnal temperature range have been documented by Dai et al. (1999) and Zhou et al. (2009), among others, but cloud cover and soil moisture trends in the tropics are very difficult to assess due to poor records. In the absence of cloudiness and soil moisture data, we shall demonstrate that precipitation-temperature relationships undergo large spatial and seasonal variations which go a long way in helping to understand actual temperature variations. Further, our hypothesis is that a better knowledge of high-frequency (and local) relationships between precipitation and temperature can shed light on lower frequency temperature variations (decadal and mutidecadal), and help in the attribution of trends.

Temperature-precipitation relationships have been examined in previous studies dealing with global climate (Trenberth and Shea 2005 ; Déry and Wood 2005 ; Adler et al. 2008 ; Berg et al. 2014). These

studies found that in many parts of the world there are significant interannual correlations between monthly temperature and precipitation, but the spatial and seasonal patterns are complex. Positive correlations tend to dominate over northern mid-latitudes in winter, and some oceanic regions in the tropics, while negative correlations dominate the mid-latitudes in summer and tropical lands. However there is a clear lack of details about this relationship in the tropics. Furthermore, most studies are restricted to monthly and annual time-scales. Studies based on daily data are few (e.g., Isaac and Stuart, 1992, for Canada) although this time-scale is better appropriated to have a glimpse of actual processes. Groisman et al (2000) shows that, even in the tropics, there are complex relationships between cloud occurrence and temperature. While a cooling effect is generally found, cloud cover result in warmer conditions at nighttime in the winter hemisphere, a moderate nighttime warming also seems to occur at mountain sites all year round, but based on a small data sample (Groisman et al. 2000). We shall further explore this issue and demonstrate the usefulness of lead-lag relationships of the daily temperature and rainfall data.

Our study will be devoted to the Greater Horn of Africa (GHA), including Tanzania, Kenya, Uganda, Sudan, South Sudan, Ethiopia, Eritrea, Djibouti and Somalia. There is still a very imperfect knowledge of temperature variations and trends in this part of Africa. Yet, the mountainous environment results in strong temperature gradients, with a range from hot tropical lowlands (either wet or semi-arid) to afro-alpine montane climates, and an associated variety of ecosystems. The distribution range of a number of species is strongly temperature-dependent, and this extends to parasites and their vectors, like Plasmodium spp. and some mosquitoes of the Anophele genus, which transmit malaria. Temperature is suspected to have a strong influence in the increase of malaria outbreaks in several parts of the East African Highlands in the last decades (Stern et al., 2011 ; Omumbo et al., 2011), although some controversies still exist on the magnitude of the temperature rise. Temperature variations also affect water requirements of crops (e.g., Rosenzweig et al., 2014). Hence, a better understanding of the causes and patterns of temperature variations and trends in the region is an important challenge.

King'uyu et al. (2000) found large geographical variations in observed temperature trends across eastern and north-eastern Africa, with some neighboring locations at times showing opposite trends. Over Ethiopia, Fazzini et al. (2015) found a +1.1°C increase in both maximum and minimum temperature from 1980 to 2010, although an average of 8 stations with longer records (1953-2010) shows that the rate of minimum temperature increase is twice that of maximum temperature. Christy et al. (2009), based on a thorough analysis of 100-yr of data across Kenya and Tanzania, including an adjustment for station inhomogeneities in the time-series, noted strong minimum temperature increases but much lower for maximum temperature whose rising became substantial only in the last (1979-2004) sub-period. They interpreted the differences between maximum temperature (Tx) and minimum temperature (Tn) trends as a response to complex changes in the boundary layer dynamics, with Tx being influenced by the daytime vertical connection to the deep atmosphere whereas Tn represents only a shallow layer. For Uganda, Christy (2013) also demonstrated much stronger temperature rises for Tn than for Tx across the twentieth century. Omondi et al. (2014) focused on temperature and precipitation extremes. They found them to be quite spatially consistent for both day-time and & night-time temperatures, but not for precipitation.

A drying trend for the boreal spring season in the eastern part of the GHA has been documented by Lyon and Dewitt (2012) and Funk et al (2012). Williams et al. (2011) also reported a precipitation decrease in June-September over much of the summer-rainfall area of the Greater Horn of Africa (Sudan, western Ethiopia, Uganda) between 1948 and 2009. In Ethiopia, Mekasha et al. (2013) noted that trends of temperature and precipitation extremes vary considerably among stations located within a given eco-environment. However, a significant drying trend (1960-2002) is found for the main rainy season (June-

September) over several watersheds of south-western Ethiopia (Cheung et al., 2008). In Djibouti, Ozer and Mahamoud (2013) found a strong decline precipitation over the period 1966-2011, and a parallel temperature increase. For Sudan, Elagib and Mansel (2000) found a significant warming between 1941 and 1996 in the central and southern parts of the country, and noted that the period of greater warmth coincided with that of rainfall depletion reported in the post mid-1960s. Maps of recent (1979-2010) temperature trends across Africa (Collins, 2011, her figure 5) actually show that significant trends basically occur in the parts of the continent experiencing seasonal dryness, whereas within the rainbelt trends are weaker and insignificant. This result suggests that a full interpretation of temperature trends need to take other climate variables, such as cloudiness or rainfall, into consideration. A separate analysis of maximum and minimum temperatures may also be desirable (Lobell et al 2007; Christy et al., 2009).

The study consists of three steps. First, the association between rainfall occurrence and temperature variations on a daily basis is examined. It is hypothesized that this will shed light on the indirect role played by cloudiness and evaporation on temperature. Maximum and minimum temperature will be separately considered, and the spatial and temporal patterns of the relationship will be carefully analyzed. The lead-lag aspects of the relationships will also be investigated. Second, long-term temperature trends (1953-2013 and 1973-2013) will be presented, at regional and local scales. At local scale, possible differences between temperature trends associated with wet and dry days will also be examined. Third, trends in rainfall occurrence will be studied. Any such trend may impact temperature trends given the hypothesized relationships between temperature and rainfall occurrence on a daily basis. A method will be defined to remove the contribution of variations in rainfall occurrence on temperature, and the subsequent adjusted temperature trends will be analyzed.

2. Data and methods

The study area comprises all countries belonging to the Greater Horn of Africa (GHA) sub-region (namely Djibouti, Eritrea, Ethiopia, Kenya, Somalia including Somaliland, Sudan, Tanzania and Uganda), between 8°S and 21°N, and 29°E and 52°E. However, Sudan's westernmost part, Tanzania's southernmost part, Burundi and Rwanda are not included. The analyses rely on the local comparison of temperature and precipitation variations. They only consider observed station data, since there are still some inconsistencies within numerical simulations (therefore possibly in reanalyses) in their reproduction of temperature-precipitation relationships (Stuart and Isaac 1994 ; Trenberth and Shea, 2005 ; Berg et al., 2014), and global gridded products are unable to document the sharp climatic gradients found in the GHA.

2.1 Temperature data

Daily maximum and minimum temperatures (Tx and Tn, respectively) are extracted from two main databases. The Global Historical Climate Network Daily (GHCND) data set (Menne et al., 2012) provides the longest time-series, with 29 stations having at least 30 years of data from 1953 onwards across the region. It has been supplemented by data from the Global Summary of the Day (GSOD) data set archived by NOAA (http://www1.ncdc.noaa.gov/pub/data/gsod). A few additional daily station temperature time-series from the Kenya Meteorological Department and the Somalia Water and Land Information Management unit (SWALIM) have also been incorporated.

Basic quality control has been carried out (deletion of minimum temperatures outside the [-10 to +40°C] range, and of maximum temperatures outside the [0 to +58°C] range ; detection of major jumps in the time-series based on visual inspection of deseasonalised anomalies).

For reference temperature trends, gridded maximum and minimum temperature data from the Climate Research Unit (CRU TS 3.10) data set (Harris et al., 2014) are also used. They consist of observed data at monthly timescale, interpolated on a 0.5 x 0.5 latitude x longitude grid.

2.2 Rainfall data

Daily rainfall data originates from the Centre de Recherches de Climatologie (CRC) database at Université de Bourgogne. It mostly consists of data from GHCND and from the various national meteorological organizations. A few GHCND Sudan stations have been rejected due to many outliers in the post 1990 time-series. Some data from GSOD have also been included, but after a careful check since in some years and stations reports of nil rainfall are dubious. 24-hour GSOD totals recorded on day 0 have been attributed to day -1, since the standard practice for daily rainfall is to record it at 0600 UTC (0900 East African Time) while most of the rain falls during the preceding day. This adjustment is normally already effective in data originating from national meteorological services.

2.3 Combined data set

The combined temperature and rainfall network consists of 95 stations (fig.1) representative of a wide range of elevations and climates. Mean annual maximum temperature ranges from 20.7°C at Robe (Ethiopian Highlands) to 37.9°C at Atbara (Nile Valley in northern Sudan), and mean minimum temperature ranges from 7.4°C at Robe to 26.2°C at Djibouti on the Gulf of Aden. Lowland stations of the northern GHA, from Djibouti to northern Sudan through the coasts of Eritrea, as well as northeastern Somalia, are the driest, with mean annual rainfall below 200 mm (fig.1). The plains of Somalia, eastern Ethiopia, northern and eastern Kenya are also quite dry (200 to 600 mm annually). The Ethiopian Highlands, the Great Lakes area and parts of the Kenya and Tanzania Highlands are relatively wet, with mean annual rainfall in the range 1000-2000 mm. The Indian Ocean coast is arid along Somalia, and becomes wetter in Kenya and Tanzania (800-1200 mm). A similar gradient is found southwards along the Nile Valley in Sudan.

The main analyses are based on the period 1953-2013, with different sets of data depending on the kind of analysis performed. The full data set, comprising stations with short duration of records, is used for the study of daily temperature anomalies associated with rain day occurrence. A more restricted network is used to analyze trends.

2.4 Methods for the analysis of the relationship between daily temperature and rainfall

For the study of daily temperature variations associated with rainfall occurrence, rain days are defined as those on which at least 1 mm precipitation is recorded. This classifies as dry days those with very light precipitation, although the accompanying cloudiness may have some effect on temperature. However, since such low intensity rainfall events are often missed out and recorded as zero rainfall, it is safer to adopt a 1 mm threshold. Maximum and minimum temperature anomalies associated with rainfall occurrence are then computed for a period of 7 days before to 7 days after the rain day. Note that this may include additional rainy days, but in the composite analyses we do not consider whether the days before or after the central day are actually wet or dry. This is due to the fact that in wet seasons / regions, it is impossible to find sequences of 15 days comprising dry days only but for the central day. The issue will however be further discussed below. Temperature anomalies are expressed as departures from the monthly temperature average. Each temperature anomaly profile, consisting of 15 days, is thus computed for each month and each station separately. No consideration is made of the period of data

availability, since the daily rainfall-temperature relationship is believed to be quite robust. However a minimum of 400 days is required for a station to be retained, and a minimum sample of 10 rain days in a month (all years together). 795 stations-months meet these requirements. The 795 profiles combining maximum and minimum temperature anomalies are classified using a k-means algorithm, based on squared Euclidean distances. For the sake of simplicity, a basic partition in 3 clusters is presented here.

To further document the relationship between rainfall and temperature and take into account the role of both rainfall occurrence and intensity with a lead time of up to 4 days, stepwise multiple linear regression (MLR) models are defined, for each station, with daily temperature as the dependent variable and a set of 10 potential predictors describing rainfall. Five of them are binary ("dummy") variables describing rainfall occurrence from the day of temperature recording (d0) to 4 days before (coded 1 for a rain-day of at least 1 mm, and coded 0 for a dry day). Five additional predictors describe rainfall amounts for the same days. Note that there is an evident covariation between rainfall occurrence and rainfall amounts. However, in most cases the attempt to use as predictors occurrence only, or amounts only, resulted in significantly lower skills of the MLR models, hence both variables were kept. Additionally, there is a rationale for considering separately rainfall occurrence and amounts. While rainfall occurrence may be seen as a rough proxy for cloudiness, rainfall amount impacts soil moisture, thus implying two different driving mechanisms for temperature variations (i.e., through the radiative balance and latent heat flux, respectively). Variables reaching the 0.95 significance were added iteratively to the MLR models, until the addition of other predictors did not further improve the model. This was done on a monthly basis, to factor out the effect of the seasonal cycle. The multiple regression is devised for explanatory purposes only, not prediction, therefore no cross-validation is carried out.

2.5 Methods for trends analysis

Temperature trends are next investigated at both regional and local scales. At regional scale, a temperature index for the GHA is computed over the period 1953-2013 by spatially averaging temperature anomalies of all stations having at least 4 years of data. Note that all anomalies are computed with respect to the period 1961-1990, used as reference, even if the station data do not fully cover this period. To do that, CRU temperatures for the grid-point nearest to each station are extracted. The difference D between the CRU mean temperature recorded on the years Y for which data are available at the station and the 1961-1990 mean CRU temperature is computed. Local (station) temperature anomalies with respect to 1961-1990 are then retrieved by adding D to the locally–derived anomalies for years Y.

Trends in spatially-averaged temperatures are investigated through least square linear regressions. In order to assess the reliability of the trends thus obtained, and of the choices made in data averaging, a comparison is made with the CRU temperature data extracted for the grid-points nearest to the stations. Note that it is inadequate to compute separate regional (GHA average) temperature indices of wet-days and dry-days since the temperature – rainfall relationships differ between stations (see below).

Local trends (for each station) are determined over the period 1973-2013, over which the space-time data availability is best. Over this period, 30 to 70 stations are available each year. In any given year, only stations-months for which at least 3 wet and 3 dry days are available are used. Other years are set to missing. These apparently low thresholds actually account for interannual variability in wet and dry days frequency, and for dry seasons / locations at which rain occurs only on a few days (for instance, the mean number of rain days in semi-arid northeastern Kenya during April, the wettest month, is as low as 5 to 7 days out of 30 days). Similarly, in very wet seasons / stations, there are not many dry days. From the initial data base, only 22 stations with at least 20 years of data can be retained. Least square linear

regressions are then applied to monthly mean maximum and minimum temperature, separately for wet and dry days. Note that a one-day lag is considered between temperature and the rainfall occurrence / absence (see results on lag-composites under section 3.1).

Trends in rain day frequency (RDF) and rainfall amounts are next computed. RDF is the ratio between the number of wet days and the number of days available. This was used to account for the existence of isolated days with missing temperature and/or rainfall records. In order to assess the effect of temperature data availability, trends based on both all rainfall data and days with available temperature information were compared.

Finally, the possible influence of rainfall trends on temperature is examined. The method is based on the stepwise multiple linear regression (MLR) models computed earlier. Daily temperature variations explained by rainfall occurrence and amounts from day 0 to day-4 are computed. The daily residuals of temperature from these models are used to depict temperature variations free from the contribution of precipitation change. Monthly mean temperatures are then computed from these residuals, and are subject to local trend detection using least-square regressions over the years 1973-2013. These trends are compared to those found for raw mean monthly temperatures, in order to determine whether temperature trends are weaker / enhanced after extracting the contribution of rainfall trends.

Note that a parallel method based on daily rainfall occurrence only has been used. The temperature of a wet day at a given station was converted to that of a “pseudo-dry day”, by adding the average difference between wet and dry days for the corresponding month and station. The same procedure was carried out to take into account lead-lag relationships between rainfall occurrence and temperature. The general results were fairly similar to those obtained from the stepwise MLR, but with this method it is uneasy to assess the combined contribution of rainfall occurrence during several consecutive days, therefore only the MLR results are presented.

Another simpler method to assess the temperature trends free from the rainfall contribution has been defined using monthly mean temperature and rainfall at each station. Temperatures were linearly regressed against monthly precipitation, and the trends in the residuals were compared to those obtained from the raw temperature time-series. It will be shown (section 3.4) that the results are broadly similar to those obtained with the above method. Although this latter method is simpler, the one based on daily time-series will be preferred since this time-scale provides useful information on the possible mechanisms and the timing of the interactions between rainfall and temperature.

3. Results

3.1 Daily temperature variations associated with rainfall occurrence

The 3 types of daily temperature anomaly profiles retained from the k-means analysis are displayed on figure 2 (top panel, Tx). All show a decrease in maximum temperature associated with the rainfall event, with a magnitude much weaker for cluster 2 (-0.7°C) than for clusters 1 and 3 (about -1.3°C). Also note the asymmetry of the profiles : the cooling generally peaks one day after the rain occurrence, except for cluster 1 where anomalies are similar on day 0 and day +1. The return to average temperature is slow for all types, while before the rainfall event a small temperature anomaly can be found on day -1 only (clusters 1 and 3).

The 3 clusters are much more strongly differentiated by their minimum temperature profiles (fig.2, Tn). Cluster 1 is associated with a warming, peaking at +1.2°C on day 0, and a relatively symmetrical pattern

suggesting a gradual warming before the rainfall event and a gradual cooling after that. On the contrary, cluster 3 displays a decrease in minimum temperature, which is however short-lived, peaks on day +1 (-0.7°C) and shows no precursor signal. Cluster 2 has a flat temperature profile, with a very small rise of minimum temperature mirroring the small decrease of maximum temperature.

Four sample stations illustrating clusters 1 and 3 are presented in figure 3. Thick lines denote temperature anomalies from 7 days before to 7 days after a rainfall event of any intensity, while thin lines consider events recording over 10 mm only. Meru and Nairobi (cluster 1 in April), in the highlands near Mount Kenya, show a typical pattern of reduced maximum temperature (-0.5 to -0.8°C one day after a rainfall event of any intensity) and increased minimum temperature (+0.3 to 0.4°C). For maximum temperature, there is clear persistence of negative anomalies long after the rainfall event. Increased cloudiness may explain both the increased minimum temperature (through reduced outgoing longwave radiation) and the decreased maximum temperature (decreasing incoming shortwave radiation), although for the latter additional cooling may result from evaporation of surface soil moisture, even some time after rainfall occurred. It is noteworthy that these anomalies (especially for Tx) are larger, reaching -1°C, when the composite is restricted to the >10mm precipitation events, suggesting that the cooling effect is stronger after a more intense precipitation. The occurrence of some significant (though weaker) anomalies before day 0 is explained by the fact that not all rain events occur as isolated rain days. Garissa and Wajir (cluster 3 in April) are also located in Kenya but in the eastern lowlands. The climate is hotter and drier, although April is the peak rainfall month of the MAM rainy season. A marked cooling is found for maximum temperature (around -1.2°C on day +1). Maximum temperature is also significantly below normal on the day of the event, and after day +1 (around -0.5°C). Minimum temperature also deviates significantly form normal, but negatively, contrary to what found in the highlands, and for a shorter period of time than for maximum temperature. It is suggested that these Tn anomalies mainly reflect surface cooling associated with increased evaporation, since a change in cloudiness would more likely result into higher minimum temperature. Like at the two other stations, temperature anomalies are larger when selecting only heavy (>10mm) precipitation events.

The spatial patterns of the 3 types of temperature profiles are actually far from random (fig.2, bottom panels). Type 3 tends to occur at low elevation, in the dry areas, especially during the MAM and OND rainy seasons in northeastern Kenya, eastern Ethiopia and Somalia, in central Sudan during the early part of the JJAS rainy season. It is also found all around Lake Victoria in January (relatively dry season) and at some locations in western Ethiopia in April. As suggested above, it is hypothesized that the decrease of both Tx and Tn mainly reflects surface cooling associated with short-lived disturbances, increased evaporation, in hot environments. By contrast, type 1 is mostly associated with highland stations (mainly Ethiopian and Kenya Highlands above 1500 m), except from July to September where it is superseded by cluster 2. The Tn increase is suggested to reflect increased cloudiness, associated with larger-scale disturbances, sometimes actually present before the precipitation event itself. Interactions with mid-latitude systems in the boreal winter and spring seasons are known to contribute to rainfall occurrence during these seasons in Eritrea, Ethiopia and sometimes as far as Kenya (Habtemichael and Pedgley 1974 ; Okoola 1989 ; Camberlin and Philippon, 2002). An alternative hypothesis is that precipitation events accompany synoptic-scale cold air advection, although near the equator the temperature change related to this mechanism is likely to be small. Finally, cluster 2 is found in more diverse environments: in the highlands during boreal summer (July-September), in the lowlands (e.g., eastern Kenya) in the dry seasons, in central Sudan in the second part of the JJAS rainy season (not shown) as well as along the Indian Ocean coast from July. With the exception of dry season lowland stations (where rainfall events are rare and of low intensity), this mostly corresponds to locations where convective rainfall dominates, but in rather moist environments (e.g., late in the rainy season). It can be hypothesized that the daytime cooling effect (Tx) is reduced because the surface is already moist.

Similarly, the nighttime cooling is reduced and compensated by a higher cloudiness, resulting into virtually no signal in Tn.

Although the above mechanisms are speculative only, these results clearly show that the temperature response to rainfall occurrence is not unique. A decrease of maximum temperature is generally found shortly following a wet event, but its magnitude and durability varies both spatially and seasonally. The response of minimum temperature is even more contrasted, with both cooling (drier lowland stations) and warming (cooler highlands stations). An important outcome is that the commonly used diurnal temperature range (DTR) is an ambiguous variable, whose variations cannot be properly interpreted without separately considering the behavior of maximum and minimum temperature.

While the strongest association between rainfall occurrence and temperature is at one-day lag, significant temperature anomalies are often found several days after the rainfall event. To further document this issue, as well as the role of rainfall intensity, stepwise MLR models are defined, for each station and each month, which relate daily temperature on day 0 to precipitation occurrence and and rainfall amounts, for day 0 to day -4. Figure 4 shows which predictors are picked up in the regression models (at the 0.95 significance level), as a percentage of all models (stations), for the GHA as a whole. For Tx, predictors depicting rainfall occurrence are those retained most often, especially on day 0 and day -1. In the wet months of April and October as much as 75-85% of the models pick up both rainfall occurrence and rainfall amounts. However, a large percentage of the models additionally retain rainfall occurrence in the preceding days (day -2 to day -4, each one being picked up in about 60% of the April models). Rainfall amounts have a generally smaller contribution, but still explain part of the temperature variance unaccounted for by rainfall occurrence. While the amount on day 0 is generally of little relevance, that on day -1 contributes much more, and at longer lead times amounts may even have a larger contribution than occurrence (e.g., see day -4 in October). The right parts of the panels in figure 4 show the distribution, for all the stations sampled, of the multiple correlation coefficient between temperature and the precipitation predictors, in the stepwise models. In the MAM and OND seasons, the median multiple correlation is close to 0.5. This indicates than in half the stations, at least 25% of the Tx variations can be explained by rainfall from day -4 to day 0. As a result, precipitation variations cannot be ignored in the interpretation of temperature variations and trends.

The same analysis is carried out for minimum temperature (fig.5). Predictors are mostly restricted to day 0 and day-1. The incidence of precipitation events before day -2 is generally small or negligible. Multiple correlations are lower than for maximum temperature, indicating that precipitation explains a smaller part of minimum temperature variations, but day-to-day variations of Tn are damped compared to those of Tx.

3.2 Temperature trends

Interannual variations and long-term trends of temperature for GHA as a whole are shown in figure 6, for the years 1953-2013 and on a seasonal basis (seasons are defined here based on the overall rainfall regimes). The comparison with the CRU data shows that the two data sets are consistent. Despite the gaps in the daily temperature records, and the uneven spatial distribution of the stations, the time-series correlate at 0.79 to 0.90 for Tx and 0.81 to 0.85 for Tn. Linear trends are also very similar between the two data sets, with those based on station data differing from the CRU data by no more than 0.03°C/decade. All seasons show warming trends, for both Tx and Tn. Based on our data set, minimum temperature increased at a high rate (+0.20 to +0.25°C/decade). The trend in maximum temperature is slightly weaker, but still strong (+0.17 to +0.22°C/decade). These values are close to or slightly above those found by Collins (2011) for mean temperature over Africa as a whole in the period 1979-2010.

Only marginal differences are found between seasons, although the northern summer (June-September) shows the largest warming trends for both Tn and Tx over GHA.

Regional trends mask out some local variations. Local trends are examined over the period 1973-2013 using a smaller network of stations, enabling a separation of wet and dry days (fig.7). The frequency distribution of Tx and Tn trends shows that, for all seasons and stations combined, dry days tend to exhibit a slightly stronger warming than wet days, but the difference is relatively small. Median Tx trend for the 22 stations used in this analysis is at +0.16°C/decade for wet days, and +0.20°C for dry days. For Tn, which shows an overall stronger warming than Tx, the difference is slightly larger (+0.25 and +0.32°C/decade for wet and dry days respectively). Seasonally (fig.7, bottom), the difference between the Tx trends of wet and dry days is largest in January-February and October-December ; it is absent in the two other seasons. For Tn, the differences are more consistent, dry days experiencing a stronger warming throughout the year. In apparent contradiction to figure 6, January-February exhibits the strongest Tn warming, but this is biased by the fact that much of the GHA except its southernmost part is dry during this season, hence only stations in the south could be used to compute the differential wet day and dry day trends, whereas in figure 4 all GHA stations and a longer period (1953-2013) are used.

Maps of local trends are presented in figure 8 (only the MAM and OND seasons are displayed). They confirm that the differences in trends between wet and dry days are generally not big. In MAM and at most stations, Tn trends following dry days are slightly stronger than those obtained for wet days. The same applies to Tx trends in OND. Although trends are not strongly different in the northern and southern parts of the GHA, there are larger local discrepancies between neighboring stations. However, trends for dry days tend to be spatially more uniform, whereas for wet days sharper spatial variations prevail in the amplitude and sign of the trends (see Tx in both MAM and OND on fig.8).

As an example of how temperature variations differ between wet and dry days, the stations of Garissa (eastern drylands of Kenya) and Nairobi Airport (Kenya Highlands) are extracted, for OND 1973-2011 (fig.9). Both common features and discrepancies emerge. The two stations are illustrative of the fact noted over the GHA that Tn shows a more upward trend than Tx. Garissa actually shows a small Tx decrease in the period. In both stations, the trends for wet and for dry days are quite consistent. However, trends for wet days generally show a slightly smaller increase (and a larger decrease for Tx at Garissa) than trends for dry days. This is again illustrative of the results obtained for the GHA as a whole. Other interesting features are the larger interannual variations obtained for Tx than for Tn, and the wider gap between wet and dry days in the maximum than in the minimum temperatures. As noticed above (section 3.1), an outstanding feature is that wet days at lowland, dry locations (e.g., Garissa) tend to result into lower temperatures for both Tx and Tn, whereas at highland stations (e.g., Nairobi) only Tx is below normal, while Tn is above normal.

On the whole, several of the above results indicate that wet occurrences markedly affect temperatures in the GHA. This is obvious at daily time-scale, although geographical variations do occur in the way temperatures are impacted. There also appears to be some differences in the long-term temperature trends when dry and wet days are analysed separately. Spatially more consistent temperature trends are often obtained when considering only dry days. The next step is therefore to look for possible changes in rainfall frequency, and whether they could affect temperatures.

3.3 Trends in rainfall frequency and amounts

Trends in the frequency of rain days (RDF) are computed on a monthly and station basis. In order to match the study of temperature trends, the period of study is restricted to 1973-2013. A minimum

number of 15 daily observations per month is needed to compute RDF, and at least 30 years of data to compute trends. 40 stations satisfy this requirement (no stations in Sudan). The number of stations having simultaneous daily temperature data is smaller (13, mainly in Kenya). To assess the representativeness of these stations, a comparison is made between the RDF trends based on the whole rainfall data set and the trends based on the stations having both rainfall and temperature data ("restricted network").

Figure 10a shows the distribution of monthly RDF trends (all stations and months together). It is almost symmetrical, with both positive and negative trends and a median close to zero (no trend). However, 7.5% of the months and stations do show a positive trend exceeding +2.5% per decade (i.e., over 10% increase in rain days over 1973-2013), and 12.9% of the series show a negative trend below -2.5% per decade. The distribution of trends based on all data is quite similar to that of trends based on the restricted network. This gives confidence on the use of the restricted network to document rainfall trends in the region. Figure 10b shows the mean in RDF trends across the GHA region on a monthly basis. Negative trends dominate the period from February to September. The rainfall decrease is largest in April-May, reflecting the current drying trend found over the region during boreal spring (Lyon and Dewitt, 2012 ; Funk et al., 2012). October and November singularize by a marked increase in rainfall occurrence. Nicholson (2015) also noted a higher October-November rainfall between 1997 and 2012 compared to the earlier years.

Figure 10 shows that trends based on the restricted network quite adequately mimic those obtained from the full network, although in some months (e.g., December) there are noticeable discrepancies. Trends in RDF are also compared to those observed for monthly rainfall amounts averaged over the GHA, available for a much larger number of stations (fig.10b, dashed line with crosses). The seasonal trends are fairly consistent, again with the exception of December. This makes us believe that, for the most part, results based on the restricted network provide a fair view of the actual trends for GHA as a whole.

The spatial patterns of the RDF trends by season (fig.11) confirm the marked decrease in rain day frequency in March-May, over most of the GHA region. Negative RDF trends also dominate in January-February, although weaker and more erratic. A quite consistent decrease is found during the June-September period as well, mostly over Uganda, Ethiopia and western Kenya, although some stations depart from this pattern. October-December trends are mostly positive, with the largest increases over Kenya and Tanzania. Note the negative trends over Uganda are more uncertain due to the incomplete GSOD rainfall data in the 1990s and 2000s. However, some negative rainfall trends over the last decades have been documented by other studies (Lyon and DeWitt, 2012 ; Williams et al., 2012 ; Liebmann et al., 2014). Diem et al. (2014), based on 1983-2012 African Rainfall Climatology version 2 (ARC2) rainfall estimates, also found decreasing rainfall over Uganda, but (unexpectedly) due to decreasing intensities rather than a change in rainfall days.

Trends in mean monthly rainfall amounts (fig.12) are fairly similar to those of rainfall occurrence. There is a balance between positive and negative trends. Positive trends dominate in the period from October to January while negative trends dominate between February and May. In some months, especially June and July, there is less agreement between the trends depending on the data sets used in the computation, as a result of greater spatial variations than in the rest of the year. Otherwise, even the restricted network of stations (for which both daily temperature and precipitation data are available) is adequate to portray general trends over the region. The spatial patterns of the trends in rainfall amounts are quite similar to those of RDF and are therefore not presented.

3.4 Temperature trends adjusted for the contribution of rainfall change

There is evidence of a superimposition, in some areas and seasons, of temperature and precipitation trends over the period 1973-2013. This is the case over Kenya and Ethiopia in March-May for example, where both a warming and a drying up are noticed (fig.8 and 11). Given the relationships found at daily time-scale between temperature and rainfall occurrence, an attempt is made to quantify the contribution of the rainfall trend to that in temperature. The temperature signal at daily time-scale associated with rainfall occurrence and intensity, as described in section 3.1, is extracted from the raw daily temperature data (see methods under section 2.5). Monthly temperature values are then computed from both the raw temperature data and the adjusted (contribution of precipitation trend removed) temperature data.

Taking the station of Nairobi-Airport as an example, figure 13 displays interannual variations and linear trends of mean April (top panel) and November (bottom panel) maximum temperatures. April raw Tx shows a marked warming trend (+0.25°C/ decade). April is also characterized by a strong precipitation decline. After correcting the daily Tx data from precipitation contribution (basically, drier conditions resulting into higher Tx), the temperature trend is still positive but much weaker (+0.03°C / decade). In November reciprocally, raw Tx shows a weak negative long-term trend (-0.02°C/decade ; fig.13, bottom) . However, this is partly the result of a general increase in precipitation. Removing the precipitation change contribution gives a warming of +0.13°C/decade. This example shows that, at some stations and in certain months, precipitation trends interfere with those of temperature. The precipitation contribution can be either an increase or a decrease of temperature trends.

For April, figure 14 shows for each station the raw maximum temperature trends (left panel), the temperature trend resulting from changes in precipitation amounts (central panel, and the residual temperature after the effect from precipitation trends is deducted (right panel). At many stations, especially in Kenya, the drying up noted in April translates into a warming, explaining part of the raw temperature increase. After deducting the precipitation contribution, Tx trends are generally weaker. However, the warming is still obvious. Inter-station variations in trends magnitude are quite strong, but an interesting fact is that the variability in Tx trends slightly reduces when adjusted Tx temperatures are used instead of raw data. The same is actually found in all other months, except January. This is suggesting that part of the spatial variations between stations in temperature trends is related to local peculiarities in precipitation variability.

These analyses have been repeated for all months, for both Tx and Tn. The results are summarized in figure 15, which shows the average temperature trends across all the available stations in the GHA (1973-2013, bold red lines, showing coefficients of regression in °C per decade). These are merely rough estimates of temperature trends for the sub-region as a whole since the distribution of available stations is uneven, with Kenya being over-represented. The plots distinguish trends obtained from raw temperature data (solid lines) and those obtained from adjusted data (after removing the rainfall contribution, dashed lines with stars). The precipitation trend is also plotted. For Tn, there is little difference between the raw and adjusted temperature trends. This is because the contribution of precipitation on minimum temperature is generally smaller and less persistent than on maximum temperature. The contribution may also be either positive or negative depending on the location and season (section 3.1). Therefore, when averaged over the GHA, these effects tend to cancel out. For maximum temperature, the contribution of precipitation trends is stronger. In several months (mainly from February to July), decreasing precipitation trends have a warming effect. However, though noticeable, this effect is small (0.01 to 0.06°C/decade) compared to the overall magnitude of the warming (+0.15 to +0.26°C/decade). The months of October and November distinctly stand out as a

period where, reciprocally, warming rates tend to be negatively impacted by the precipitation trends. This season has become wetter in the recent decades over much of the GHA, impacting maximum temperature. Adjusted Tx trends tend to be slightly higher (+0.02 to 0.03°C/decade) after deducting the cooling effect associated with enhanced rainfall. For the year as a whole, precipitation trends have a detectable but small contribution on Tx trends (adjusted trend +0.156°C/decade against +0.168°C/decade for the unadjusted trend), but no effect on Tn trends.

Trends (raw and adjusted from precipitation contribution) have also been computed but based on monthly means and a simple regression extracting the contribution of precipitation variations from the monthly temperature, instead of using daily data and a multiple regression model as above. The trend coefficients are broadly similar (fig.15, thin green lines), although on individual months there are discrepancies due to the fact that the number of days to compute monthly means is not always the same from year to year. The main observation is that the extraction of rainfall variations from the temperature signal leads to the same conclusion as when using daily data. A noticeable effect of rainfall trends on temperature coefficients is found mostly for Tx, during months in which the precipitation trend is most obvious (lower trend coefficients in April-June, as rainfall has decreased, and higher trend coefficients in October as rainfall has increased). However, the difference between the raw and residual trends is, as above, quite small. This result suggests that monthly data could be used to extract the effect of precipitation variations from temperature time-series, although working on daily data enables to better understand the likely processes at work.

4. Conclusion

The composite analyses presented in this study showed that in most of the GHA there is a clear relationship between rainfall occurrence (>= 1mm) and daily temperature, with temperature anomalies associated with the wet events being usually highly significant. Maximum temperature generally displays a distinct cooling, peaking one day after the rainfall event, but there is often a persistence of negative Tx anomalies long after the rainfall event. The independent contribution of passed rainfall events to Tx variations (sometimes up to 4 days earlier) is confirmed through multiple regression. The amplitude of the Tx response is also often proportional to the rainfall amount. Minimum temperatures show a weaker and spatially contrasted response to rainfall occurrence. In some regions (mostly cool highland areas) rainfall occurrence is associated with above normal Tn. In other regions (especially lowland, hot environments) it results in below normal Tn. The Tn anomalies are also much less persistent than for Tx. The spatial variations in the sign of the Tn signal and the amplitude of the Tx signal are suggested to reflect different mechanisms of the rainfall-temperature association. Given these results, it should be noted that the commonly used diurnal temperature range (DTR) is somewhat ambiguous, since it cannot be properly interpreted without separately considering the behavior of maximum and minimum temperature and their respective relationship with other weather variables such as rainfall and cloudiness.

These rainfall-temperature relationships should first be interpreted as the effect of cloudiness on net radiation. Increased cloudiness may explain both the increased minimum temperature at many stations (through reduced outgoing longwave radiation) and the decreased maximum temperature (decreasing incoming shortwave radiation). However, the temporal asymmetry of the Tx cooling with respect to the rainfall event suggests that in addition to the cooling associated with cloud cover, the persistent soil moisture anomaly resulting from the precipitation event also contributes to cooling. This is confirmed by the fact that the cooling is stronger when the rainfall events are heavier. Another finding is that the nighttime warming associated with rainfall occurrence (and supposed increased cloud cover) is not ubiquitous. In some cases (mainly hot climates, in the early part of the rainy season), a Tn decrease (not

increase) is found which tends to replicate, with damped anomalies, the pattern found for Tx. This could simply reflect the fact that starting out from a lower Tx would result in a lower Tn during the following night, even if the nighttime decrease was to be the same as on dry days. However, it is suggested that these Tn anomalies, given the overall dry and hot environment (contrary to what found in the highland areas and at the end of the rainy season), could also reflect surface cooling associated with increased evaporation. This hypothesis would be in line with Koster et al. (2006) and Miralles et al. (2012) who demonstrated that the soil moisture-temperature coupling is highly variable in space and time. Miralles et al. (2012) found that a stronger coupling is expected in transition zones between wet and dry climates, as well as at times of soil moisture deficit and high atmospheric water demand. This is typical of the early part of rainy seasons in the GHA lowlands. These variations in the temperature signal associated with rainy events, either in space (e.g. highlands vs lowlands) or in time (e.g. between the early and late parts of the rainy season, as in June-September in Sudan for instance) indicate that, even in tropical environments, any overgeneralization on the interpretation of temperature variations and trends should be avoided.

These remarks are of relevance when analyzing climate change, especially temperature trends. Most of the GHA show warming trends, for both Tx and Tn and with marginal differences between seasons. From 1953 to 2013, minimum temperature increased at a high rate (+0.20 to +0.25°C/decade depending on seasons, for a GHA average). The trend in maximum temperature was only slightly weaker (+0.17 to +0.22°C/decade). When dry days and wet days are analyzed separately, and for all stations and seasons combined (over the period 1973-2013 to account for rainfall data availability), dry days tend to exhibit a slightly stronger warming than wet days. Other findings are the larger interannual variations obtained for Tx than for Tn (a feature found in most of the tropics ; see for instance observations made at Khartoum, Sudan, by Elagib, 2011), and the temperature gap between wet and dry days being wider for the maximum than the minimum temperatures.

By contrast to temperatures, monthly trends in both rainfall occurrence and amounts since 1973 show quite symmetrical distributions, with a balance between positive and negative trends. Trends in rain days exceeding 10% between 1973 and 2013 are found at 7.5% and 12.9% of the months and stations for positive and negative trends, respectively. The largest negative trends in rainfall occurrence and rainfall amounts are found in April-May over most of the region, in agreement with Lyon and Dewitt (2012) and Funk et al. (2012). By contrast, a distinctive increase in rainfall occurrence and rainfall amounts is found in October-December.

In parts of the GHA and some seasons, rising temperatures in the last 40 years therefore coincide with (increasing or decreasing) precipitation trends. Given the response of both Tx and Tn to rainfall occurrence at daily time-scale, regression models are used to extract the rainfall influence on temperature variations, accounting for lag effects up to 4 days. The daily residuals of temperature from these models are used to depict temperature variations free from the effect of precipitation variations. Trends computed on the monthly means of these residuals are then compared to those found for raw mean monthly temperatures. At stations where the rainfall trend is strong, removing the rainfall contribution results in noticeable changes in linear temperature trends (either enhancement or attenuation).

However, at the scale of the GHA as a whole, these effects do not strongly modify the sign and magnitude of the warming in the last 40 years. In the February-July period, adjusted maximum temperature trends after removing the contribution of the generally downward rainfall trend show a slightly reduced warming (+0.18°C/decade on average, instead of +0.21°C/decade for raw Tx data). On the contrary, the Tx increase in October-November is slightly attenuated by the positive rainfall trend

found at this time of the year. On the whole the removal of the rainfall contribution tends to smooth out the seasonal pattern of Tx trends, resulting in a more uniform warming across the year. For Tn, adjusting for rainfall contribution has virtually no impact on the overall temperature trends. This results from the fact that rainfall occurrence is associated with either an increase or a decrease of temperature depending on the location and time of the year.

Precipitation trends, although they only have a marginal effect at the scale of the GHA, are to be taken into account in the attribution of temperature trends. As pointed out by Trenberth and Shea (2005), neither temperature nor precipitation records should be interpreted without considering their strong covariability. They noted that warming in the United States has partly been lessened due to increases in cloudiness and precipitation, with more energy going into evaporation and less into sensible heating. Besides the effect of cloud cover and surface moisture on temperature, a warmer atmosphere and land surface impact the water cycle, including precipitation rates (Held and Soden, 2006 ; Wentz et al., 2007). Although the present study does not challenge at all this assumption, neither does it underestimate the role played by energy gradients in large-scale atmospheric dynamics and associated precipitation occurrence, it also draws attention to the fact that in the tropics temperature variations are strongly dependent on rainfall. This relationship is best evidenced by separating maximum and minimum temperature, and working at daily time-scale, but it also holds at interannual time-scales (Déry and Wood, 2005 ; Berg et al., 2014). As an outcome of this dependence to rainfall, skillful projections of rainfall patterns are key to the accurate estimation of future warming at regional scale.

687 References
688

689 Adler RF, Gu G, Wang JJ, Huffman GJ, Curtis S, Bolvin D (2008) Relationships between global precipitation
690 and surface temperature on interannual and longer timescales (1979–2006). J Geophys Res 113,
691 D22104, doi:10.1029/2008JD010536.
692 Berg A, Lintner BR, Findell K, Seneviratne SI, van den Hurk B, Ducharne A, Gentine P (2014) Interannual
693 Coupling between Summertime Surface Temperature and Precipitation over Land: Processes and
694 Implications for Climate Change. J Climate 28(3), 1308-1328. http://doi.org/10.1175/JCLI-D-14-
695 00324.1
696 Boé J, Terray L (2014) Land–sea contrast, soil-atmosphere and cloud-temperature interactions:
697 interplays and roles in future summer European climate change. Clim Dyn 42:3-4, 683-699.
698 Camberlin P, Philippon N (2002) The East African March-May rainy season: Associated atmospheric
699 dynamics and predictability over the 1968-97 period. J Climate 15(9), 1002-1019.
700 Christy JR (2013) Monthly Temperature Observations for Uganda. J Appl Meteor Climatol 52, 2363–
701 2372. doi:10.1175/JAMC-D-13-012.1
702 Christy JR, Norris WB, McNider RT (2009) Surface Temperature Variations in East Africa and Possible
703 Causes. J Climate 22, 3342–3356. doi:10.1175/2008JCLI2726.1
704 Collins JM (2011) Temperature variability over Africa. J Climate 24(14), 3649-3666.
705 Dai A, Trenberth KE, Karl TR (1999) Effects of clouds, soil moisture, precipitation, and water vapor on
706 diurnal temperature range. J Climate 12:2451:2473
707 Déry SJ, Wood EF (2005) Observed twentieth century land surface air temperature and precipitation
708 covariability. Geophys Res Lett 32(21), L21414. http://doi.org/10.1029/2005GL024234
709 Diem JE, Ryan SJ, Hartter J, Palace MW (2014) Satellite-based rainfall data reveal a recent drying trend
710 in central equatorial Africa. Climatic Change 126(1-2), 263-272.
711 Elagib NA, Mansell MG (2000) Recent trends and anomalies in mean seasonal and annual temperatures
712 over Sudan. J Arid Environments 45, 263–288. doi:10.1006/jare.2000.0639
713 Elagib NA (2011) Evolution of urban heat island in Khartoum. Int J Climatol 31, 1377–1388.
714 doi:10.1002/joc.2159
715 Evan AT, Heidinger AK, Vimont DJ (2007) Arguments against a physical long-term trend in global ISCCP
716 cloud amounts. Geophys Res Lett 34(4), L04701. http://doi.org/10.1029/2006GL028083
717 Fazzini M, Bisci C, Billi P (2015) The Climate of Ethiopia. In P Billi (Ed.) Landscapes and Landforms of
718 Ethiopia, Springer Netherlands, 65-87.
719 Fischer EM, Seneviratne SI, Lüthi D, Schär C (2007) Contribution of land-atmosphere coupling to recent
720 European summer heat waves. Geophys Res Lett 34(6), L06707.
721 http://doi.org/10.1029/2006GL029068
722 Funk C, Michaelsen J, Marshall M (2012) Mapping recent decadal climate variations in precipitation and
723 temperature across Eastern Africa and the Sahel. In: Remote sensing of drought: Innovative
724 monitoring approaches, B. Wardlow, M. Anderson, and J. Verdin, Eds., CRC Press, pp.331-358.
725 Groisman PY, Bradley RS, Sun B (2000) The Relationship of Cloud Cover to Near-Surface Temperature
726 and Humidity: Comparison of GCM Simulations with Empirical Data. J. Climate 13, 1858–1878.
727 doi:10.1175/1520-0442(2000)013
728 Habtemichael A, Pedgley DE (1974) Synoptic case-study of spring rains in Eritrea. Arch Met Geophys
729 Biokl, Ser. A, 3-4, 285-296.
730 Harris I, Jones PD, Osborn TJ, Lister DH (2014) Updated high-resolution grids of monthly climatic
731 observations – the CRU TS3.10 Dataset. Int J Climatol 34: 623–642. doi: 10.1002/joc.3711
732 Held IM, Soden BJ (2006) Robust Responses of the Hydrological Cycle to Global Warming. J Climate 19,
733 5686–5699.
734 Hirschi M, Seneviratne SI, Alexandrov V, Boberg F, Boroneant C, Christensen OB, Stepanek P (2011).
735 Observational evidence for soil-moisture impact on hot extremes in southeastern Europe. Nature
736 Geosci 4(1), 17‑21. http://doi.org/10.1038/ngeo1032
737 Isaac GA, Stuart RA (1992) Temperature–Precipitation Relationships for Canadian Stations. J Climate 5,
738 822–830.

King'uyu SM, Ogallo LA, Anyamba EK (2000) Recent Trends of Minimum and Maximum Surface Temperatures over Eastern Africa. J Climate 13, 2876–2886.
Koster RD, et al. (2006) GLACE: The Global Land-Atmosphere Coupling Experiment. Part I: Overview. J Hydrometeorol 7, 590–610.
Liebmann B, Hoerling MP, Funk C, Bladé I, Dole RM, Allured D, Quan X, Pegion P, Eischeid JK (2014) Understanding Recent Eastern Horn of Africa Rainfall Variability and Change. J Climate 27, 8630–8645.
Lyon B, DeWitt DG (2012) A recent and abrupt decline in the East African long rains. Geophys Res Lett 39, doi:10.1029/2011GL050337
Menne MJ, Durre I, Vose RS, Gleason BE, Houston TG (2012) An overview of the Global Historical Climatology Network-Daily Database. Journal of Atmospheric and Oceanic Technology 29, 897-910.
Miralles DG, van den Berg MJ, Teuling AJ, de Jeu RAM (2012) Soil moisture-temperature coupling: A multiscale observational analysis. Geophys Res Lett 39, L21707. doi:10.1029/2012GL053703
Nicholson SE (2015) Long-term variability of the East African 'short rains' and its links to large-scale factors. Int J Climatol 35: 3979–3990. doi: 10.1002/joc.4259
Okoola RE (1989) Interaction between the Mediterranean meteorology and conditions over Africa. In: Seminar on Tropical Meteorology, Erice 26/9-4/10/86. WMO, Techn. Doc. n°277.
Omumbo JA, Lyon B, Waweru SM, Connor SJ, Thomson MC (2011) Raised temperatures over the Kericho tea estates: revisiting the climate in the East African highlands malaria debate. Malaria Journal 10, 12. doi:10.1186/1475-2875-10-12
Rosenzweig C et al. (2014) Assessing agricultural risks of climate change in the 21st century in a global gridded crop model intercomparison. Proc Natl Acad Sci USA 111:3268–3273
Soden BJ, Held IM (2006) An Assessment of Climate Feedbacks in Coupled Ocean–Atmosphere Models. J Climate 19, 3354–3360.
Stern DI, Gething PW, Kabaria CW, Temperley WH, Noor AM, Okiro EA, Shanks GD, Snow RW, Hay SI (2011) Temperature and Malaria Trends in Highland East Africa. PLoS ONE 6, e24524. doi:10.1371/journal.pone.0024524
Stuart RA, Isaac GA (1994) A Comparison of Temperature–Precipitation Relationships from Observations and As Modeled by the General Circulation Model of the Canadian Climate Centre. J Climate 7, 277–282.
Tang Q, Leng G, Groisman PY (2012). European Hot Summers Associated with a Reduction of Cloudiness. J Climate 25(10), 3637‑3644.
Tang Q, Leng G (2012a). Changes in Cloud Cover, Precipitation, and Summer Temperature in North America from 1982 to 2009. J Climate 26(5), 1733‑1744.
Tang Q, Leng G (2012b). Damped summer warming accompanied with cloud cover increase over Eurasia from 1982 to 2009. Environ Res Lett 7(1), 014004. http://doi.org/10.1088/1748-9326/7/1/014004
Trenberth KE, Shea DJ (2005) Relationships between precipitation and surface temperature. Geophys Res Lett 32, L14703. doi:10.1029/2005GL022760
Wentz FJ, Ricciardulli L, Hilburn K, Mears C (2007) How much more rain will global warming bring? Science 317(5835), 233-235.
Williams AP, Funk C, Michaelsen J, Rauscher SA, Robertson I, Wils THG, Koprowski M, Eshetu Z, Loader NJ (2011) Recent summer precipitation trends in the Greater Horn of Africa and the emerging role of Indian Ocean sea surface temperature. Clim Dyn 39, 2307–2328.
Zhou L, Dai A, Dai Y, Vose RS, Zou CZ, Tian Y, Chen H (2009) Spatial dependence of diurnal temperature range trends on precipitation from 1950 to 2004. Clim Dyn 32(2-3), 429‑440.

List of figures

Fig.1 : Station network for composite analysis of daily temperature, and mean annual rainfall map (1961-1990, CRU data, in mm). Filled circles indicate stations for which at least 10,000 daily temperature records are available over the period 1953-2013.

Fig.2 : Main 3 patterns of composite temperature anomalies from 7 days before to 7 days after the occurrence of a rainfall event, on a monthly and station basis, based on a k-means clustering of temperature profiles. Top panel : mean profiles ; bottom panels : spatial distribution of the 3 clusters for the months of January, April, July and October. X denotes stations and months with not enough rain days for the profile to be computed. Areas above 1000 meters are shaded.

Figure 3 : Composites of April daily temperature anomalies at two lowland stations in Kenya (Garissa and Wajir) and two highland stations (Meru and Nairobi), from 7 day before to 7 day after a precipitation event. The vertical bar indicates the reference day on which precipitation occurs. Stars show significant anomalies (P= 0.95) according to Student's t-test. Thick lines stand for precipitation events of any intensity, thin lines for precipitation exceeding 10 mm.

Figure 4 : Rainfall predictors (day 0 to day -4) selected in stepwise multiple regression models explaining maximum temperature variations (day 0), for the months of January, April, July and October. Values correspond to the percentage of models (i.e., stations) for which a given predictor is picked up. Both rainfall occurrence (left/blue bars) and rainfall amounts (right/purple bars) are used. On the right of each panel is shown a box-plot of the multiple correlation coefficients (across the models defined for all stations of the network).

Figure 5 : same as figure 4 but for minimum temperature.

Figure 6 : Trends and interannual variations of seasonal mean maximum temperature (left panels) and minimum temperature (right panels), 1953-2013, for the GHA regional index. Blue thick lines : average temperature anomaly for available stations (see text) ; red thin lines : CRU data ; upper green lines : number of stations used to compute the station index. The correlation coefficient between the station index and the CRU index is shown on top.

Figure 7 : Seasonal linear temperature trends over the period 1973-2013 for the 22 stations having long times-series, for days following a wet day (solid lines) and following a dry day (dashed lines). Left panels : maximum temperature ; right panels : minimum temperature. Top panels : frequency distribution across all stations and seasons ; bottom panels : median trends for each season.

Figure 8 : Temperature trends (1973-2013) for MAM (top panels) and OND (bottom panels), and for days following a wet day (left panels) and those following a dry day (right panels). Filled circles denote warming, hollow circles denote cooling. The size and color of the circles indicate the magnitude of trends in °C/decade.

Figure 9 : Mean OND temperature time-series for Nairobi Jomo Kenyatta International Airport (top) and Garissa, Kenya (bottom). Maximum temperatures are on the left panels and minimum temperatures on the right panels ; blue lines with circles show temperature on wet days, red lines with stars show dry days (enabling a one-day lag between rainfall and temperature). Scales for left and right panels are the same.

Figure 10 : Monthly linear trends of rain-day occurrence (RDF) over the period 1973-2013 over the GHA as a whole. (a) frequency distribution across all stations and months ; (b) mean RDF trends for each month across all stations. The different lines refer to different sets of data (see text). In (b), the change in regional mean rainfall amounts based on monthly rainfall data is also shown (dashed line with crosses).

Figure 11 : Trends in rain days frequency (1973-2013) for January-February, March-May, June-September and October-December, expressed as a percentage change per decade. Filled circles denote positive trends, hollow circles denote negative trends. The size and color of the circles indicate the magnitude of trends in percent per decade.

Figure 12 : Same as figure 10 but for monthly rainfall amounts.

Figure 13 : Interannual variations and trends of maximum temperature at Nairobi-Airport (1973-2011) : monthly means for April and November. Raw data (solid line with circles) and after correction from rainfall contribution (dashed line with stars). The upper dashed line shows rainfall variations. Straight lines are linear trends, with slopes as indicated in the legend.

Figure 14 : Trends in April maximum temperature (1973-2013) : raw Tx data (left panel), Tx trend induced from precipitation trends (central panel), and Tx trend adjusted from precipitation contribution (right panel). Filled circles denote positive trends and hollow circles negative trends. The size and color of the circles indicate the magnitude of trends in °C per decade. Note that the scale of the central panel differs from that of the two others.

Figure 15 : Monthly and yearly trends of maximum temperature (left panel) and minimum temperature (right panel) as an average over the GHA, 1973-2013, in °C per decade. Solid line with stars : raw temperature data ; dashed line with diamonds : temperature trend after removing the precipitation contribution. Bold red lines show trends obtained from daily multiple regression models, thin green lines show trends obtained from monthly simple regression. The lower line (dashed with circles) shows the precipitation trends ($mm.yr^{-1}$).

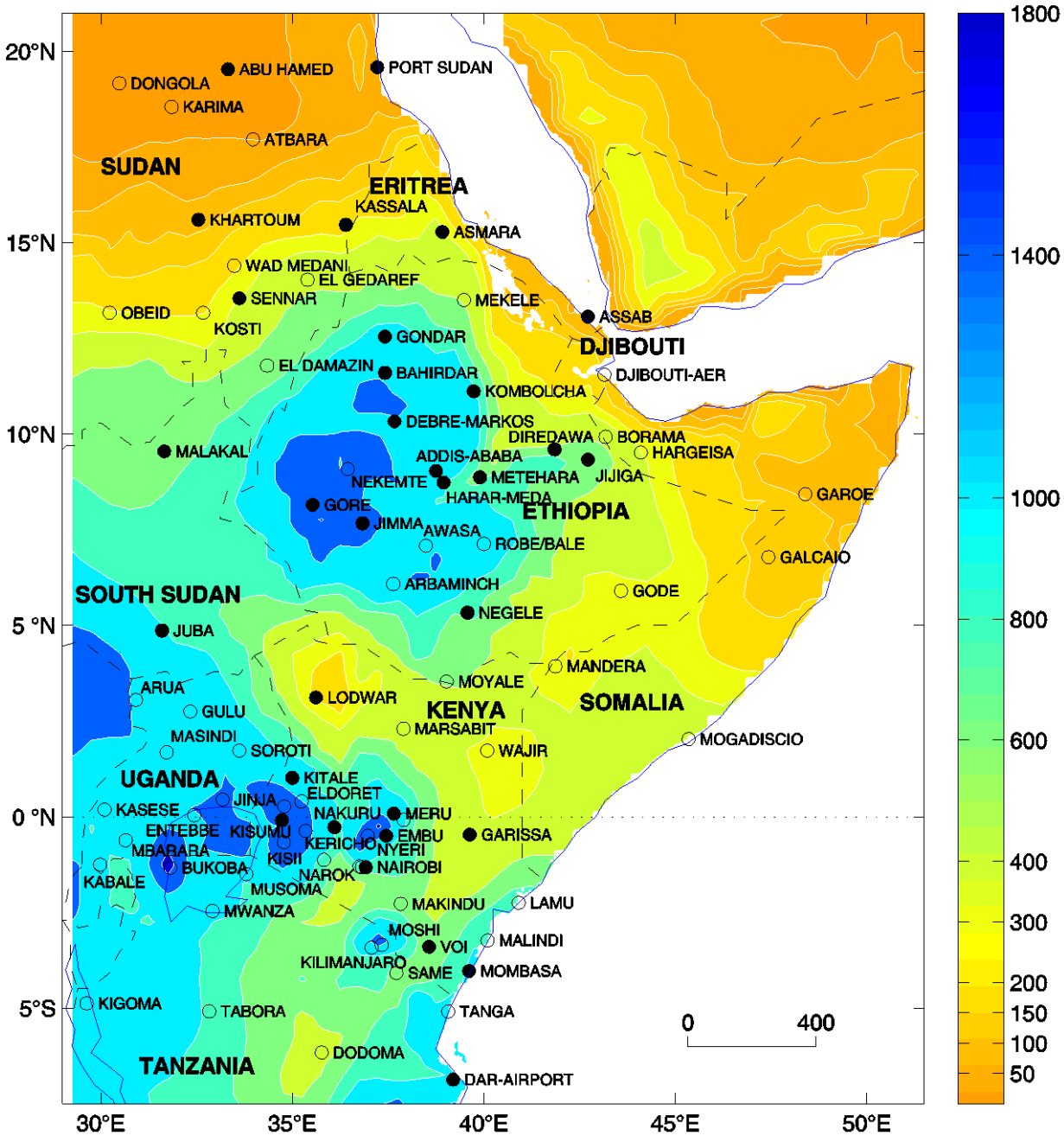

Fig.1 : Station network for composite analysis of daily temperature, and mean annual rainfall map (1961-1990, CRU data, in mm). Filled circles indicate stations for which at least 10,000 daily temperature records are available over the period 1953-2013.

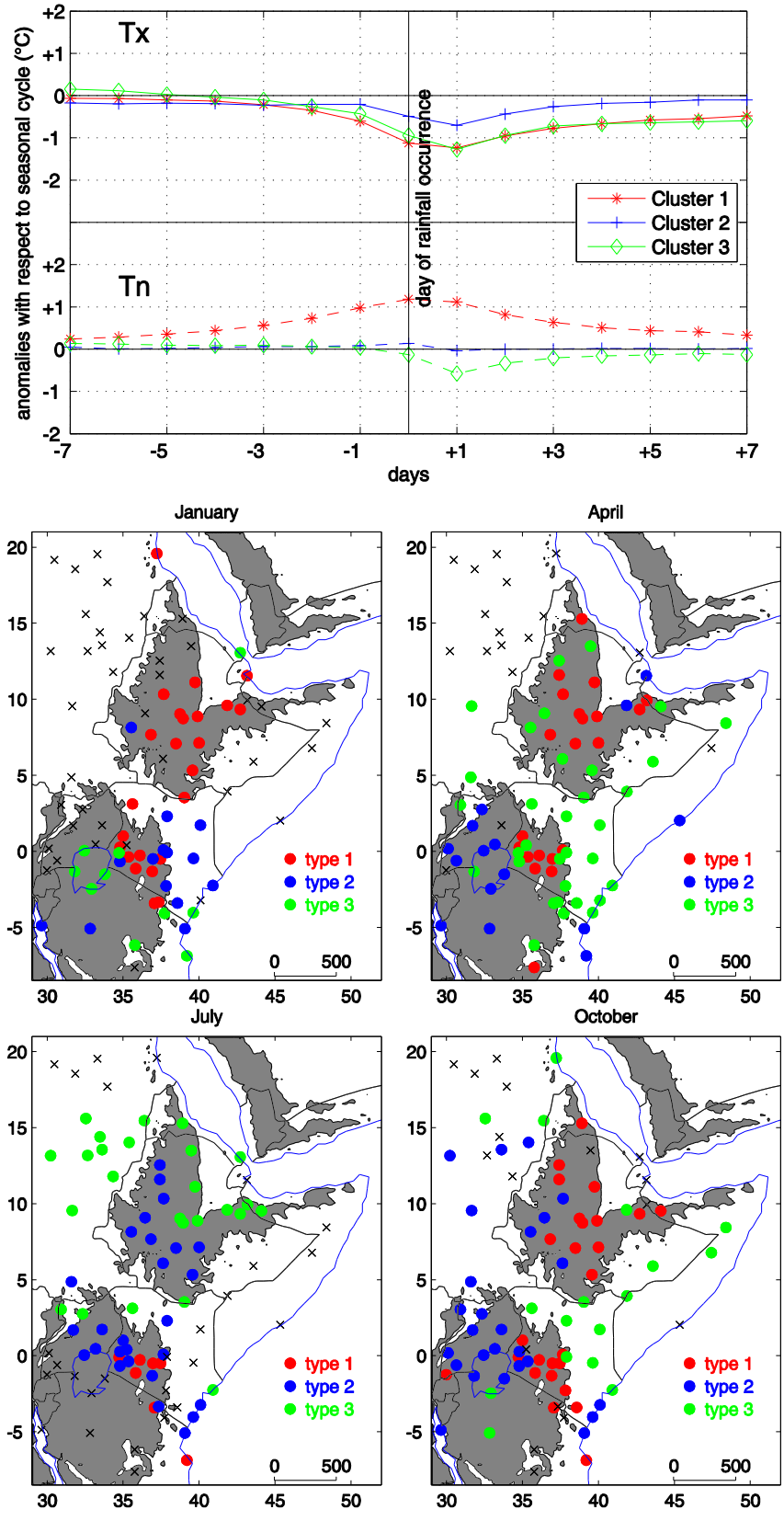

Fig.2 : Main 3 patterns of composite temperature anomalies from 7 days before to 7 days after the occurrence of a rainfall event, on a monthly and station basis, based on a k-means clustering of temperature profiles. Top panel : mean profiles ; bottom panels : spatial distribution of the 3 clusters for the months of January, April, July and October. X denotes stations and months with not enough rain days for the profile to be computed. Areas above 1000 meters are shaded.

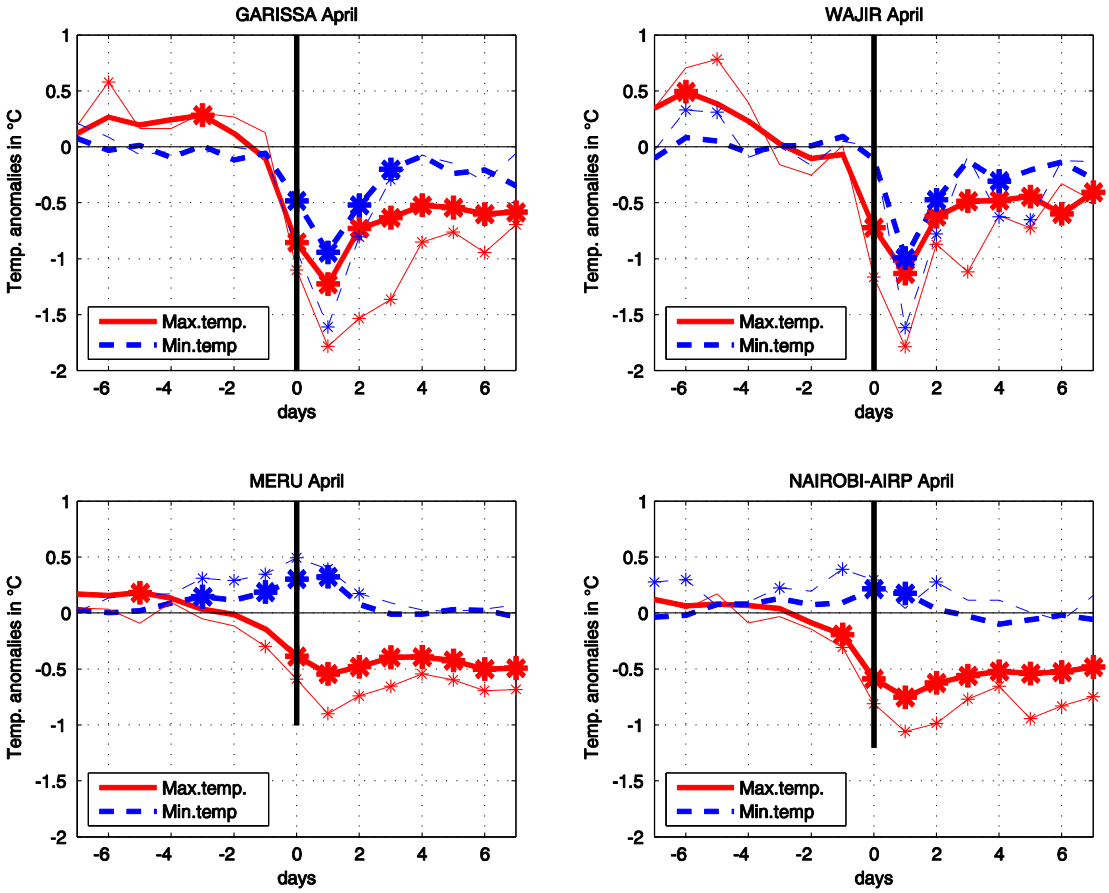

Figure 3 : Composites of April daily temperature anomalies at two lowland stations in Kenya (Garissa and Wajir) and two highland stations (Meru and Nairobi), from 7 day before to 7 day after a precipitation event. The vertical bar indicates the reference day on which precipitation occurs. Stars show significant anomalies (P= 0.95) according to Student's t-test. Thick lines stand for precipitation events of any intensity, thin lines for precipitation exceeding 10 mm.

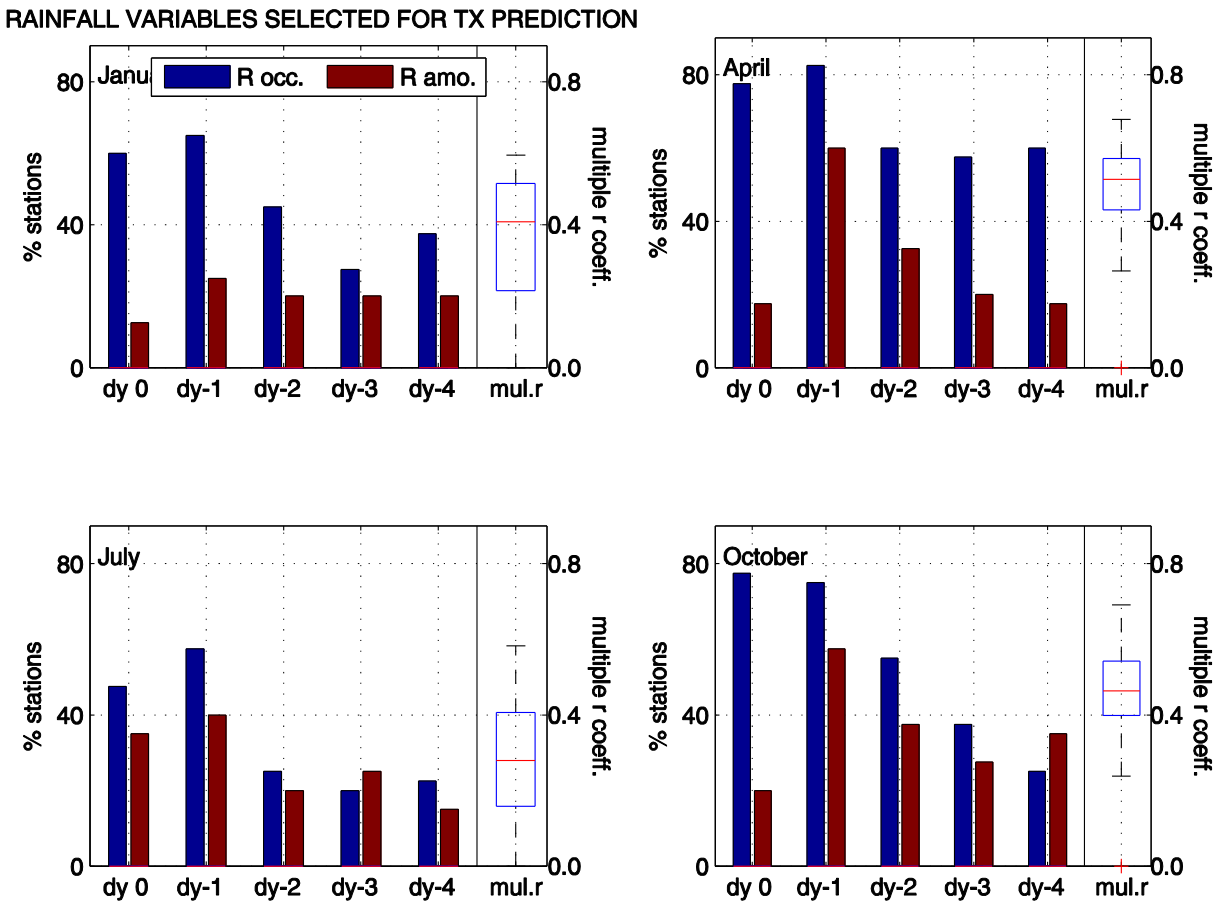

Figure 4 : Rainfall predictors (day 0 to day -4) selected in stepwise multiple regression models explaining maximum temperature variations (day 0), for the months of January, April, July and October. Values correspond to the percentage of models (i.e., stations) for which a given predictor is picked up. Both rainfall occurrence (left/blue bars) and rainfall amounts (right/purple bars) are used. On the right of each panel is shown a box-plot of the multiple correlation coefficients (across the models defined for all stations of the network).

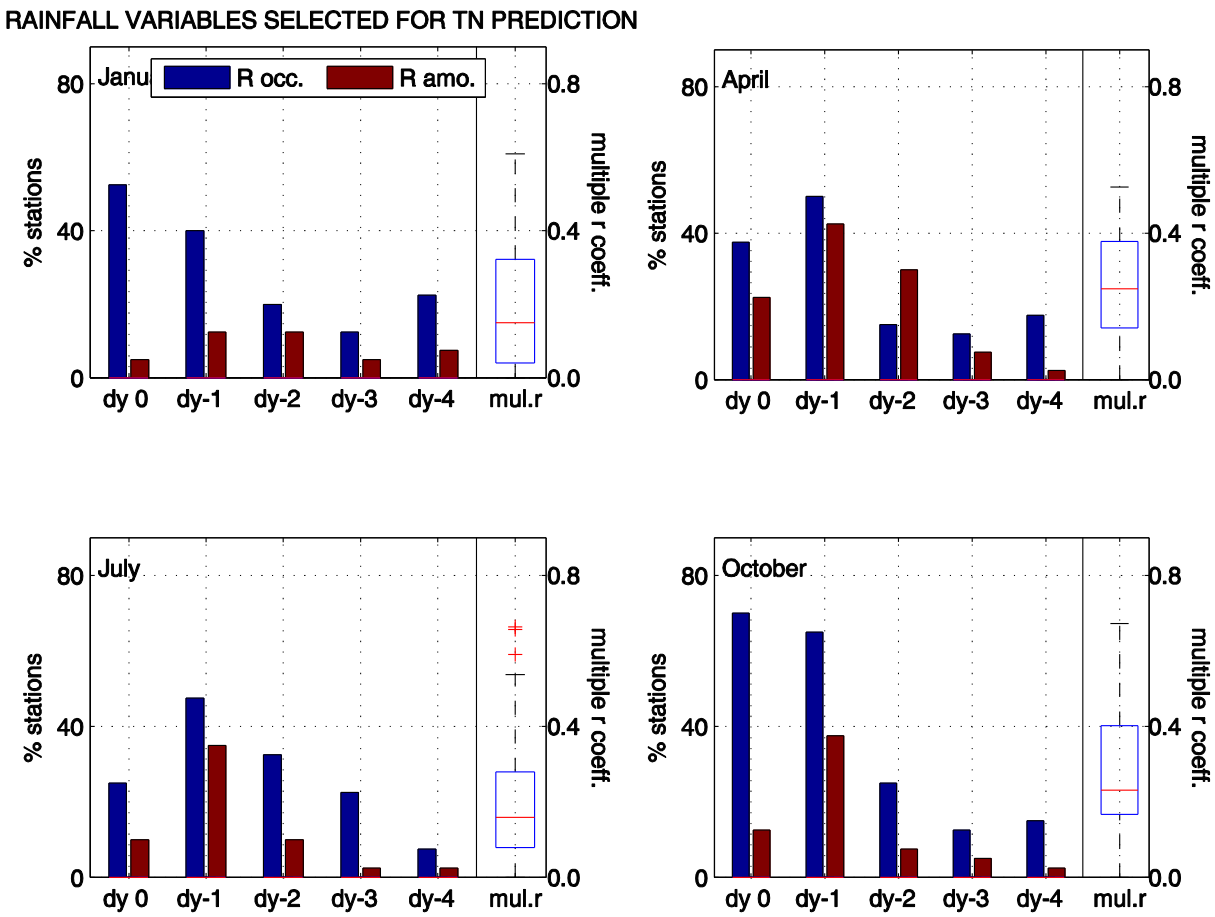

Figure 5 : same as figure 4 but for minimum temperature

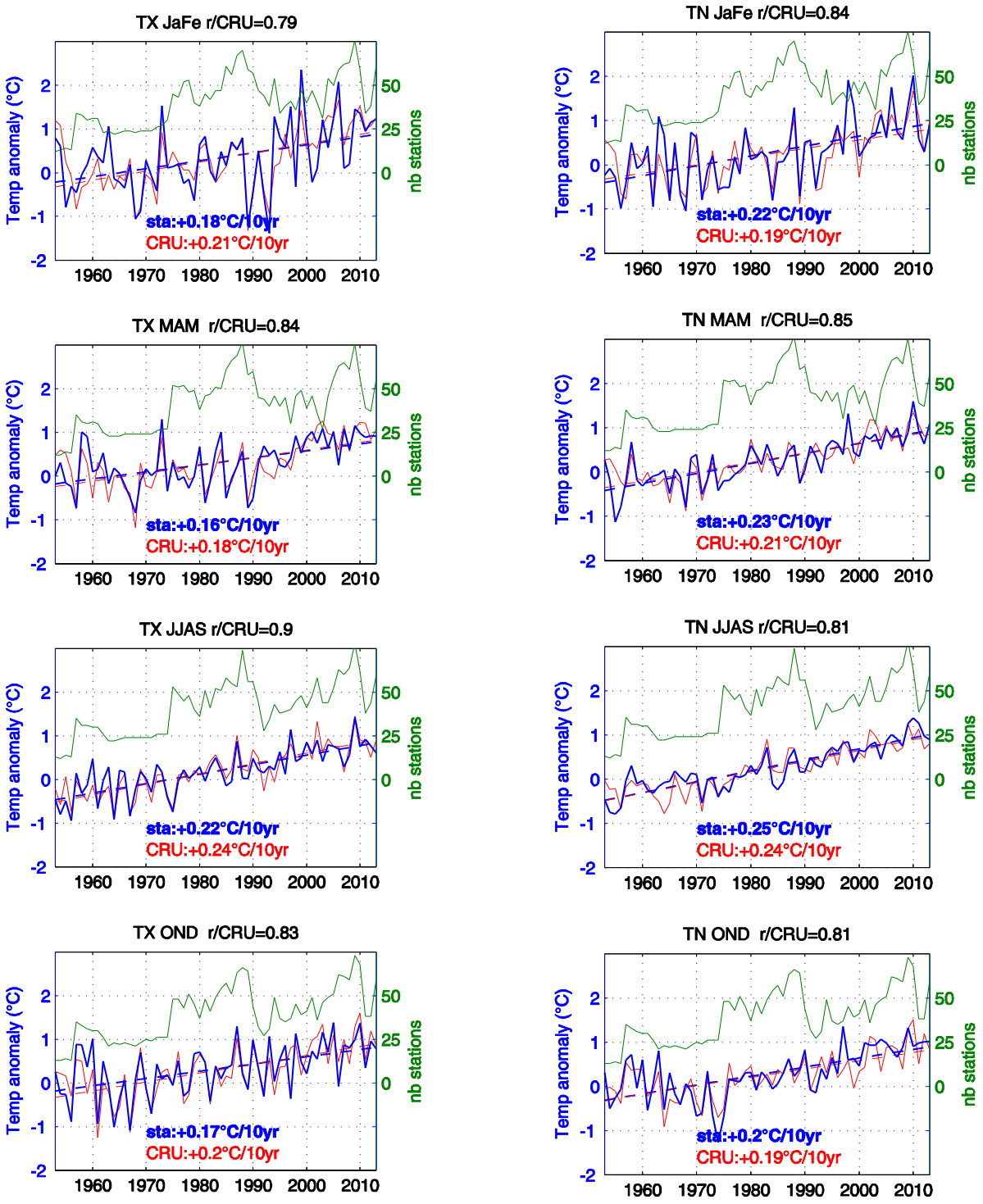

Figure 6 : Trends and interannual variations of seasonal mean maximum temperature (left panels) and minimum temperature (right panels), 1953-2013, for the GHA regional index. Blue thick lines : average temperature anomaly for available stations (see text) ; red thin lines : CRU data ; upper green lines : number of stations used to compute the station index. The correlation coefficient between the station index and the CRU index is shown on top.

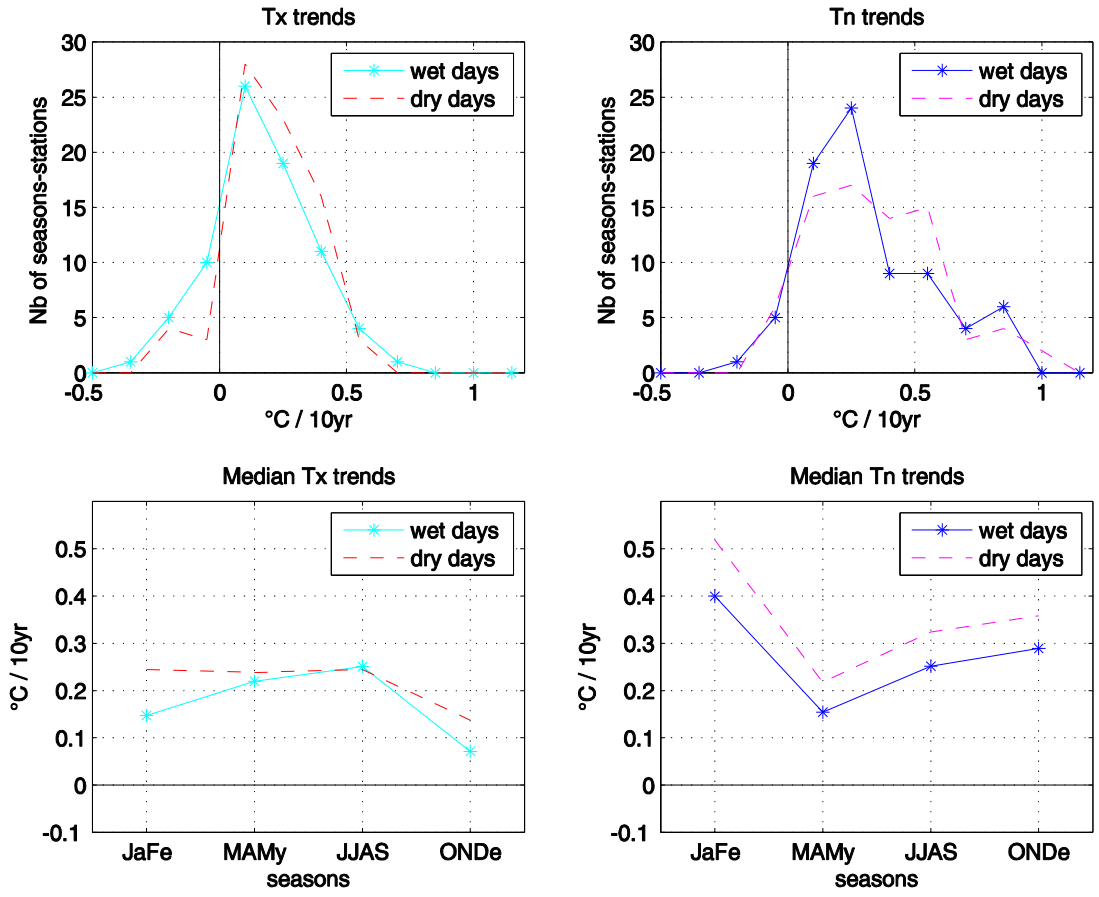

Figure 7 : Seasonal linear temperature trends over the period 1973-2013 for the 22 stations having long times-series, for days following a wet day (solid lines) and following a dry day (dashed lines). Left panels : maximum temperature ; right panels : minimum temperature. Top panels : frequency distribution across all stations and seasons ; bottom panels : median trends for each season.

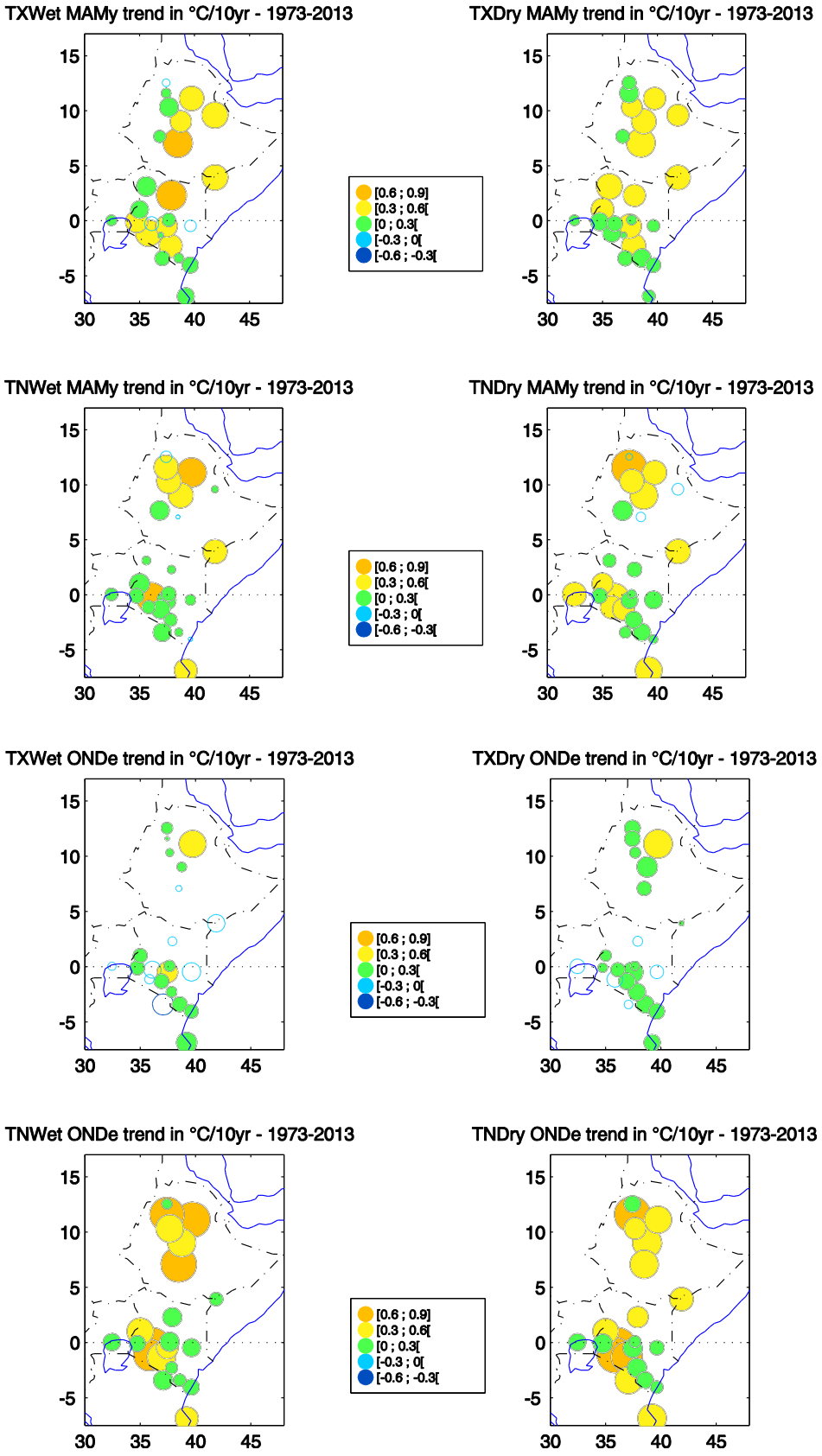

Figure 8 : Temperature trends (1973-2013) for MAM (top panels) and OND (bottom panels), and for days following a wet day (left panels) and those following a dry day (right panels). Filled circles denote warming, hollow circles denote cooling. The size and color of the circles indicate the magnitude of trends in °C/decade.

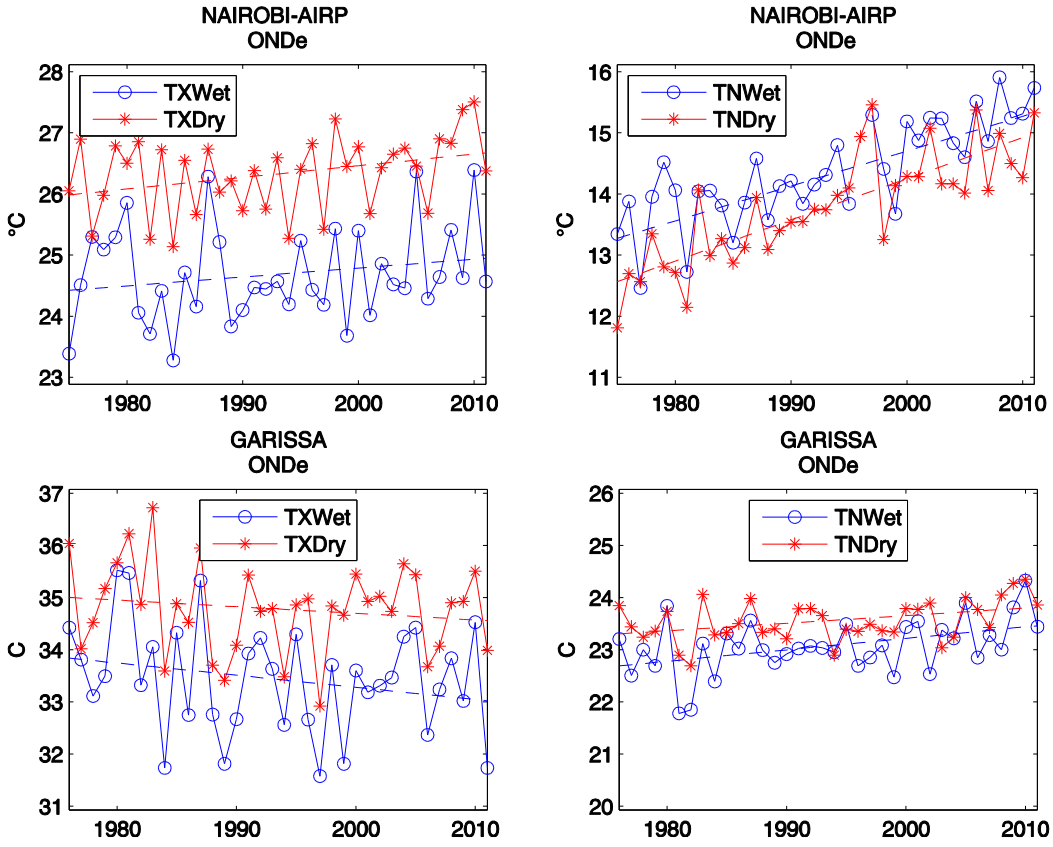

Figure 9 : Mean OND temperature time-series for Nairobi Jomo Kenyatta International Airport (top) and Garissa, Kenya (bottom). Maximum temperatures are on the left panels and minimum temperatures on the right panels ; blue lines with circles show temperature on wet days, red lines with stars show dry days (enabling a one-day lag between rainfall and temperature). Scales for left and right panels are the same.

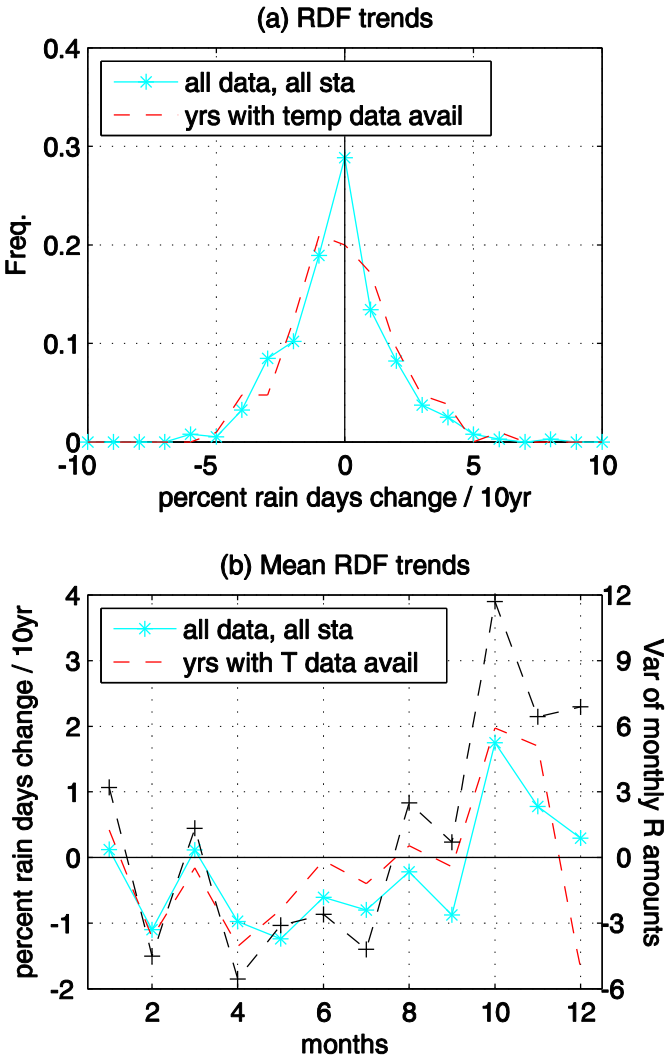

Figure 10 : Monthly linear trends of rain-day occurrence (RDF) over the period 1973-2013 over the GHA as a whole. (a) frequency distribution across all stations and months ; (b) mean RDF trends for each month across all stations. The different lines refer to different sets of data (see text). In (b), the change in regional mean rainfall amounts based on monthly rainfall data is also shown (dashed line with crosses).

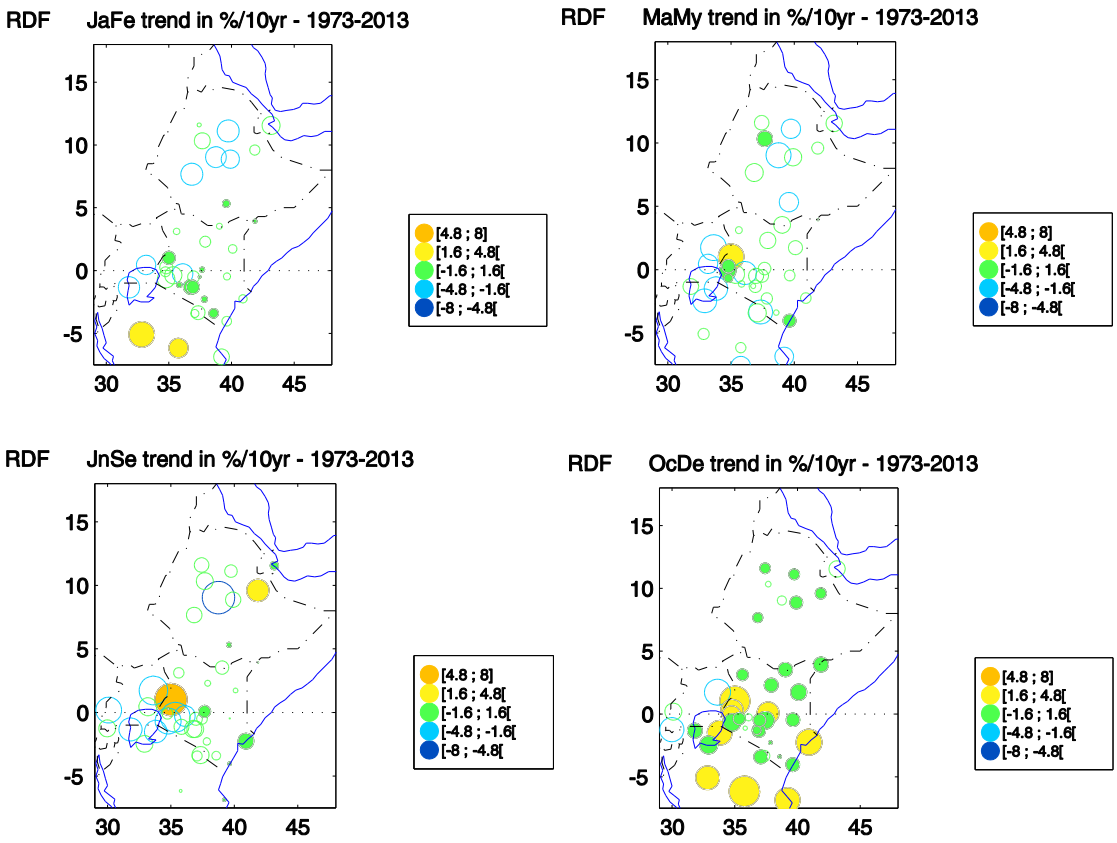

Figure 11 : Trends in rain days frequency (1973-2013) for January-February, March-May, June-September and October-December, expressed as a percentage change per decade. Filled circles denote positive trends, hollow circles denote negative trends. The size and color of the circles indicate the magnitude of trends in percent per decade.

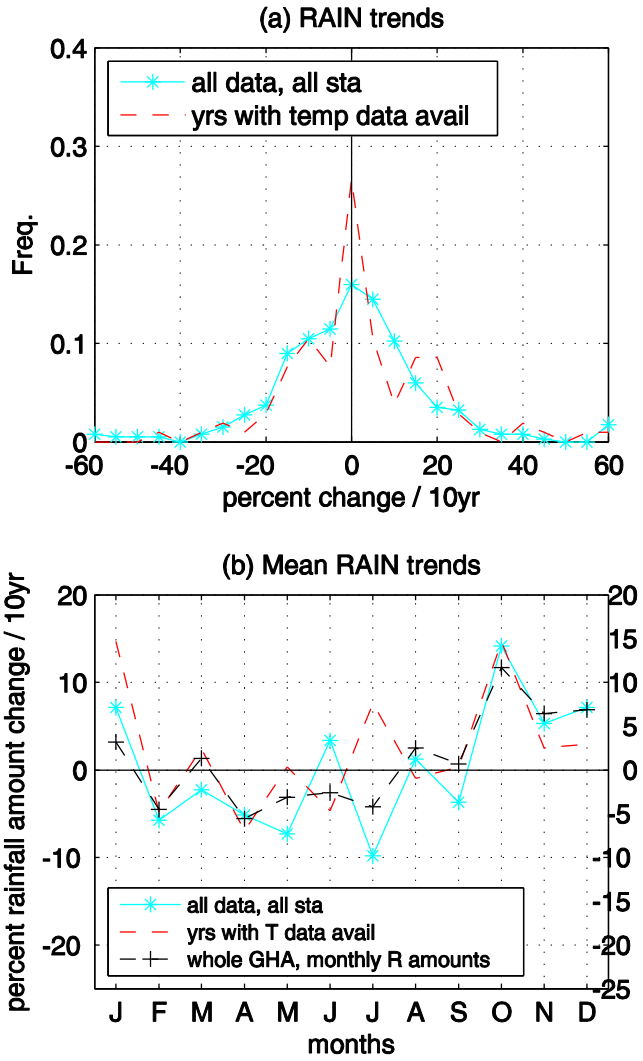

Figure 12 : Same as figure 10 but for monthly rainfall amounts

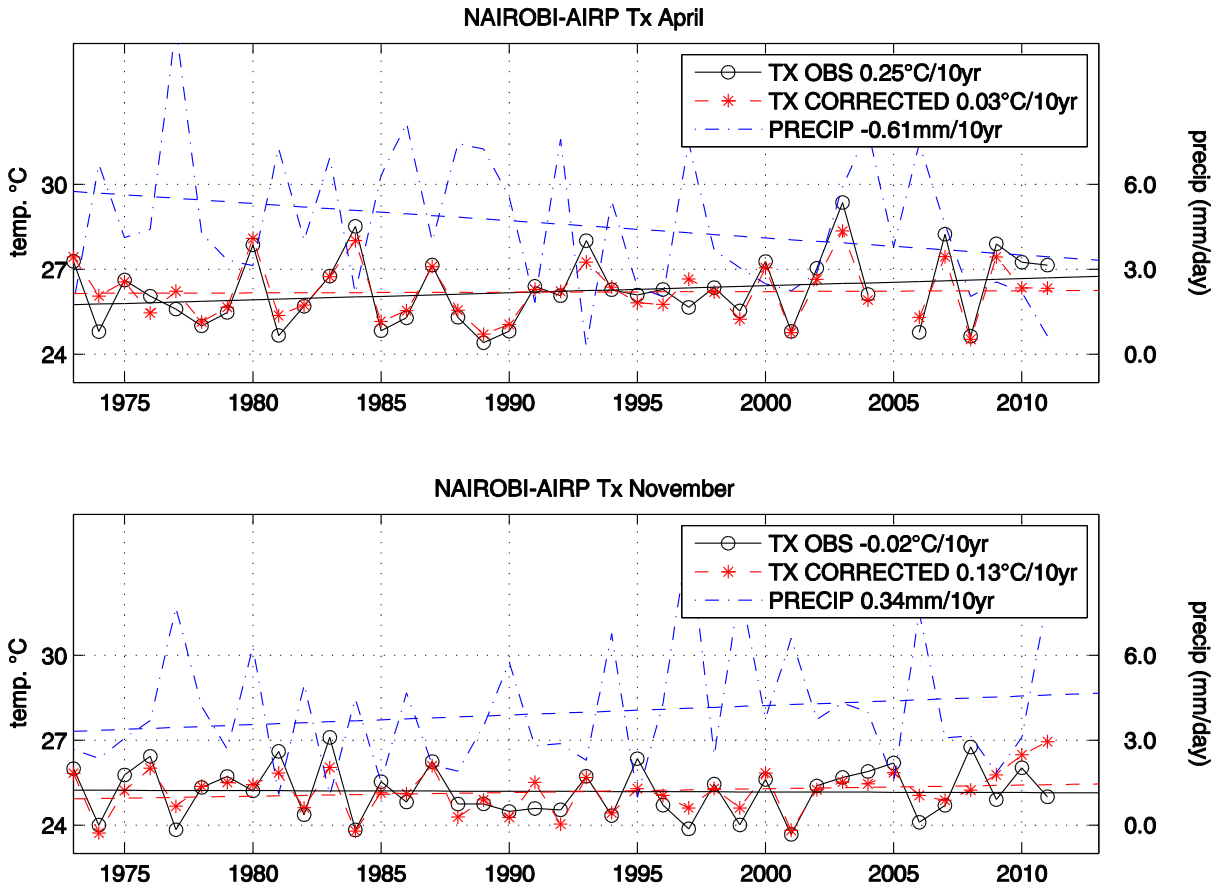

Figure 13 : Interannual variations and trends of maximum temperature at Nairobi-Airport (1973-2011) : monthly means for April and November. Raw data (solid line with circles) and after correction from rainfall contribution (dashed line with stars). The upper dashed line shows rainfall variations. Straight lines are linear trends, with slopes as indicated in the legend.

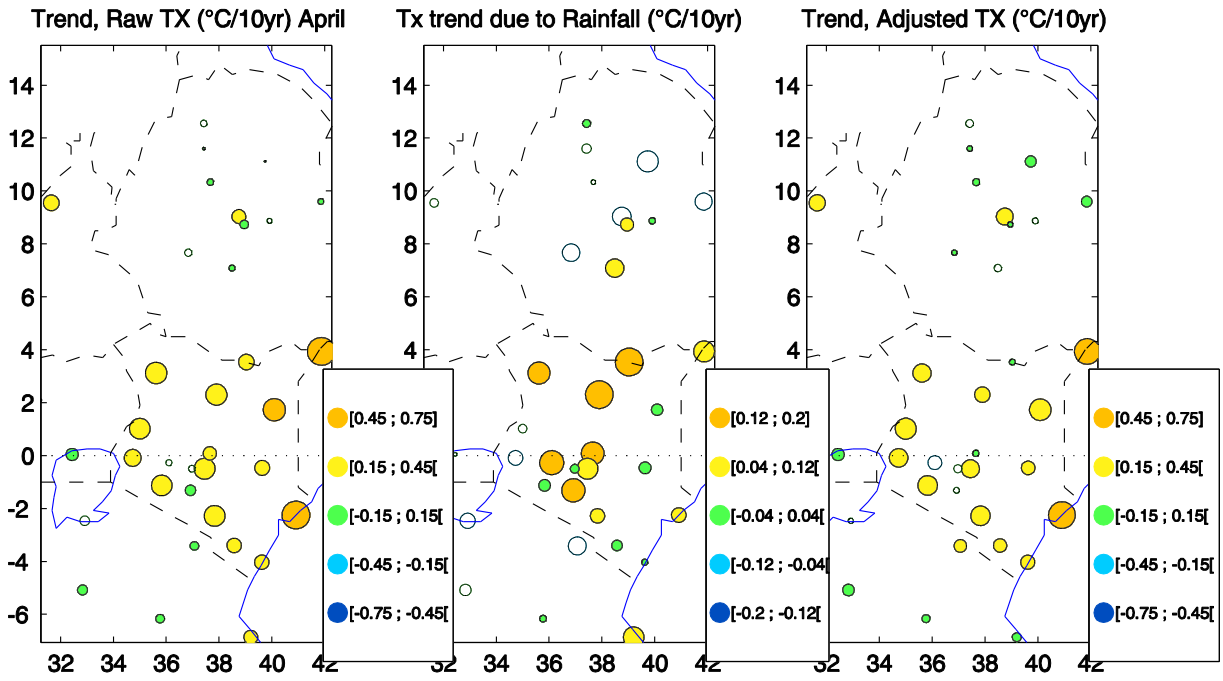

Figure 14 : Trends in April maximum temperature (1973-2013) : raw Tx data (left panel), Tx trend induced from precipitation trends (central panel), and Tx trend adjusted from precipitation contribution (right panel). Filled circles denote positive trends and hollow circles negative trends. The size and color of the circles indicate the magnitude of trends in °C per decade. Note that the scale of the central panel differs from that of the two others.

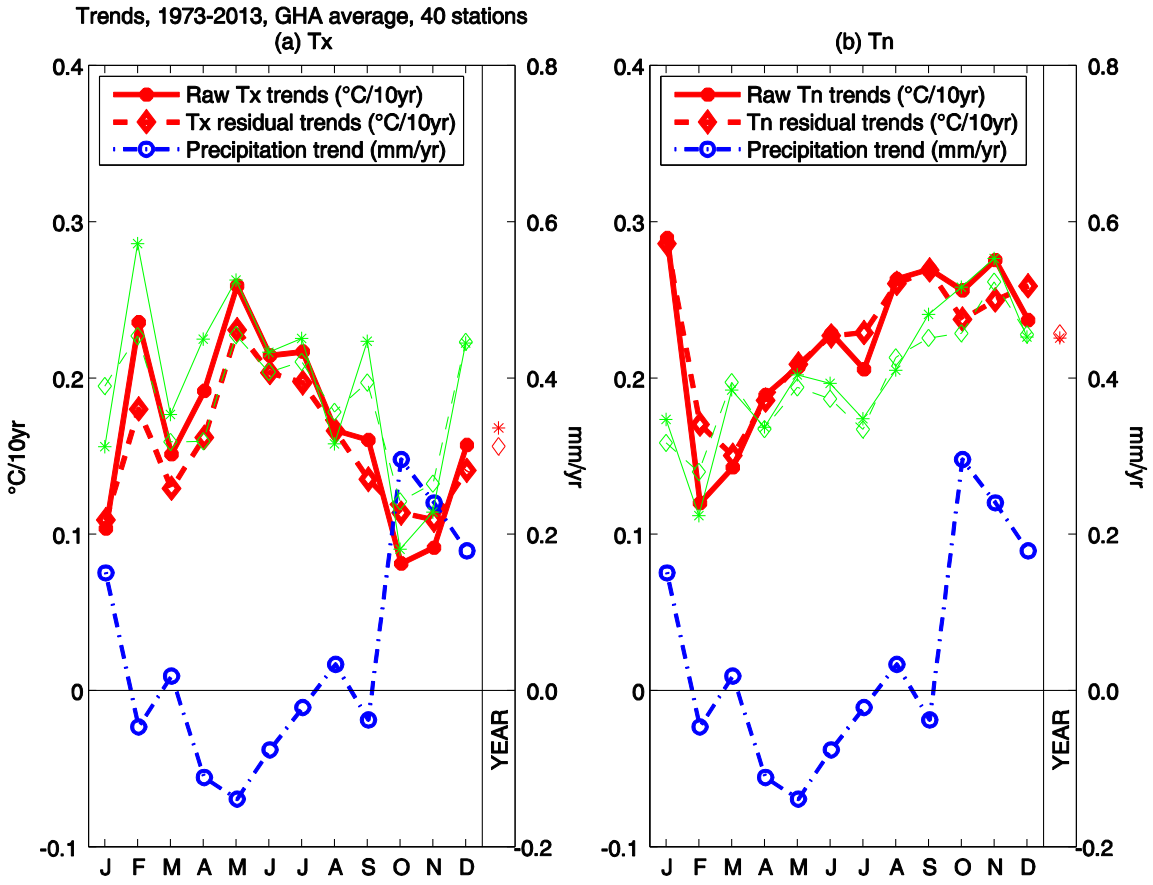

Figure 15 : Monthly and yearly trends of maximum temperature (left panel) and minimum temperature (right panel) as an average over the GHA, 1973-2013, in °C per decade. Solid line with stars : raw temperature data ; dashed line with diamonds : temperature trend after removing the precipitation contribution. Bold red lines show trends obtained from daily multiple regression models, thin green lines show trends obtained from monthly simple regression. The lower line (dashed with circles) shows the precipitation trends (mm.yr^{-1}).